*Manuscript accepted for publication

Inversion tectonics and magnetic fabrics in Mesozoic basins of the Western Tethys: a review

C. García-Lasanta[a*], B. Oliva-Urcia[b], A.M. Casas-Sainz[a], T. Román-Berdiel[a], E. Izquierdo-Llavall[c], R. Soto[d], P. Calvín[e], B. Moussaid[f], H. El Ouardi[g], J.C. Kullberg[h], J.J. Villalaín[e]

[a]*Departamento de Ciencias de la Tierra, Instituto de Investigación en Ciencias Ambientales (IUCA), Universidad de Zaragoza, Pedro Cerbuna 12, 50009 Zaragoza, Spain.*

[b]*Departamento de Geología y Geoquímica, Universidad Autónoma de Madrid, 28049 Madrid, Spain*

[c]*E2S-UPPA, UPPA-CNRS-Total, Laboratoire des Fluides Complexes et leurs Réservoirs, IPRA, Université de Pau et des Pays de l'Adour, France*

[d]*IGME, Instituto Geológico y Minero de España, Unidad de Zaragoza, 50006 Zaragoza*

[e]*Laboratorio de Paleomagnetismo, Departamento de Física, Universidad de Burgos, Spain*

[f]*École Normale Supérieure Casablanca (ENS), Université Hassan II de Casablanca, Morocco*

[g]*Dép. de Géologie, Faculté des Sciences, Université Moulay Ismail, BP 11201 Zitoune, Meknès, Morocco*

[h]*Dpto. Ciências da Terra, CICEGe, Univ. Nova de Lisboa, Qta. Torre, 2829-516 Caparica, Portugal*

[*] *Current affiliation: Geology Department. Western Washington University, Bellingham, WA 98225 USA*

Abstract

Positive tectonic inversion of sedimentary basins has been recognized as one of the primary mechanisms of mountain building and intraplate deformation. Reconstructing the tectonic history of basins is relatively easy for the inversion stage but becomes more difficult for the basinal stage, especially when strong deformation involving cleavage development is associated with the subsequent compressional tectonics. Since tectonic markers for the extensional episodes are not commonly well developed, Anisotropy of Magnetic Susceptibility (AMS) has provided recently a tool for analyzing early stages in the evolution of sedimentary basins, even in the absence of other outcrop-scale mesostructures. Here, we expose and discuss the applicability of magnetic fabrics (by means of AMS) to different types of intra-plate sedimentary basins in the Western Tethys region formed under extensional or transtensional regimes and which underwent different inversion styles (total or partial inversion, with or without cleavage development, forming part of compressional thrust sheets, etc.) owing to specific particular p-T conditions and structural controls. Factors such as lithology, magnetic mineralogy, position within the sedimentary pile and deformation intensity are key to interpret the obtained magnetic fabrics in terms of tectonic evolution. A basin classification is proposed according to inversion styles and magnetic fabrics: Where inversion did not involve cleavage development, magnetic lineation is parallel to the stretching direction corresponding to the extensional stage. The transition between non-cleaved to inversion-related cleaved units is marked by the switch of magnetic lineations from parallel to extension to parallel to the intersection lineation between cleavage and bedding. These relationships are enhanced when extension and compression are roughly coaxial, then favoring the clustering of axes of the magnetic ellipsoid. Even when extreme inversion occurs and the early, extensional fabric is obliterated, magnetic fabrics provide

information about the interaction between preferred deformation directions associated with the main stages in basin evolution.

Keywords: intra-plate sedimentary basins, inversion tectonics, AMS, magnetic mineralogy, Western Tethys

1. Introduction

Intra-plate sedimentary basins can be formed in a variety of tectonic settings, including pure extension, transtension, pure strike-slip or compression. Basin inversion is a common process in basin evolution that allows for their infill to be exposed (and, consequently, studied) at surface (Ziegler, 1982; Van Hoorn, 1987; Koopman et al., 1987). The particular evolution of sedimentary basins within a large plate or a micro-plate is crucial when defining plate kinematics, which can be strongly conditioned by their internal deformation (Cloetingh, 1988; Ziegler, 1989). Since the works by De Graciansky et al. (1989), and Williams et al. (1989), who attempted to systematize structures formed by tectonic inversion processes, their study has become a necessary routine to establish the main stages in basin evolution. In addition, new techniques (including analogue and numerical modeling, physico-chemical techniques, paleomagnetism) can be nowadays used in order to accurately characterize and differentiate processes related to either the basinal or the inversion stages (see Allen and Allen, 2013 and references therein).

The study of Anisotropy of Magnetic Susceptibility (AMS, also called magnetic fabric analysis) has become one of the most extensively used techniques in the last decades, in sedimentary, igneous and metamorphic rocks (e.g. Hrouda and Janak, 1976; Hrouda, 1982; Rochette, 1987; Borradaile, 1988; Rochette et al. 1992; Tarling and Hrouda, 1993; Borradaile and Henry, 1997; Winkler et al., 1997; Borradaile and Jackson, 2004; Parés, 2015; Bilardello, 2016). AMS has targeted, with different degree of success, the characterization of multiple geological problems: emplacement of igneous bodies (e.g. Gleizes et al., 1993; Román-Berdiel et al., 1995; Bouchez, 1997, 2000; Aranguren, 1997; Auréjac et al., 2004; Antolín-Tomás et al., 2009; Kratinová et al., 2010; Izquierdo-Llavall et al., 2012; Cañón-Tapia and Mendoza-Borunda, 2014), deformation of rocks under different P-T conditions (e.g. Parés et al., 1999; Gil-Imaz et al., 2000; Hirt et al., 2000; Robion et al., 2007; Oliva-Urcia et al., 2009; Pueyo Anchuela et al., 2012), basin evolution (Mattei et al., 1997, 1999; Cifelli et al., 2005), fold geometry and internal deformation (e.g. Aubourg et al., 1999), estimation of shallowing effect in sedimentary rocks sampled for paleomagnetic purposes (see Li and Kodama, 2016), fault rocks at shallow crustal levels (Solum and van der Pluijm, 2009; Casas-Sainz et al., 2017, 2018), paleocurrents orientation in sedimentary contexts (e.g. Rees, 1965; Hamilton and Rees, 1970; Tarling and Hrouda, 1993; Piper et al., 1996; Pueyo Anchuela et al, 2013 and references therein), etc. Multiple studies have found empirical relationships between the orientations of the magnetic and strain ellipsoids (e.g. Kneen, 1976; Wood and Gibson, 1976; Kligfield et al., 1977; Rathore, 1979; Kligfield et al., 1982; Rathore and Henry, 1982; Lüneburg et al., 1999) although their magnitudes are more complexly related and empirical relationships for different lithologies has yet to be established (Kligfield et al., 1981; Borradaile, 1987, 1988; Hirt et al., 1988; Borradaile, 1991; Lüneburg et al., 1999; Oliva-Urcia et al., 2010b).

In this sense, a number of studies about the interpretation of magnetic fabrics include correlations with magnetic and non-magnetic analyses that provide information about the minerals and their orientation distribution. Such non-magnetic analyses include crystallographic preferred orientation, CPO, shape preferred orientation, SPO (Richter et al., 1993; Lüneburg et al., 1999; Chadima et al., 2004; Schmidt et al., 2009; Hastie et al., 2011; Izquierdo-Llavall et al., 2012; Oliva-Urcia et al., 2012), distribution anisotropy (Grégoire et al., 1998; Muxworthy and Williams, 2004), or even modeled magnetic fabrics from textural data (Housen et al., 1993; Martín-Hernández et al., 2005; Biedermann et al., 2018). In addition, the magnetic anisotropy of single crystals has been also evaluated at room (Martín-Hernández and Hirt, 2003 and references therein) and low temperatures (Biedermann et al., 2014a). The AMS resulting from a combination of crystals can be also modeled, revealing the importance of the intrinsic susceptibility anisotropy of single crystals in similar rocks with similar histories but different AMS orientation (i.e., Biedermann et al., 2018). Several techniques allow separating magnetic subfabrics using remanence anisotropy (AARM, anisotropy of the anhysteretic remanent magnetization), partial remanence anisotropy, or high-field methods such as the anisotropy of the isothermal remanent magnetization -AIRM- or the high-field torquemeter measurements, including measurements at low temperature (e.g. Jackson et al., 1988; Jackson and Tauxe, 1991; Kelso et al., 2002; Lüneburg et al., 1999; Martín-Hernández and Hirt, 2001; 2004; Schmidt et al., 2007b; Martín Hernández and Ferré, 2007). However, some of these methods require further equipments in addition to the usually available in paleomagnetic and/or magnetic fabric laboratories (e.g. Ferré et al., 2004).

All in all, AMS has become of a high interest due to its broad and reliable applicability to characterize the structural context of a region where structural markers are often punctually located or scarce (e.g. Cifelli et al., 2009; García-Lasanta et al., 2015; Parés, 2015 and references therein). The possibility of characterizing the internal structure of sedimentary basins, determining the different roles of faults (with different orientations) during the inversion process, as well as predicting the orientation or location of subsoil faults from the extension directions and magnetic/deformational features obtained at surface can also promote it as a valuable tool in geological reservoirs evaluation.

In this work, we explore the applicability of AMS to intra-plate basin analysis (namely inverted extensional or transtensional basins), discussing a collection of studies developed in examples from the Western Tethys (Mesozoic-Cenozoic evolution in the Iberian and African plates; Table 1, Fig. 1). Analyzed factors include the variability of magnetic carriers, sedimentary rock types, early diagenetic processes, structures associated with extension and inversion and relationship between the strain and the magnetic anisotropy ellipsoids. We finally propose a classification according to the relationship between magnetic fabrics and major structures related to basin evolution.

2. Types of inverted basins

2.1. Extensional (basinal) stage

Intra-plate basin formation is relatively common in continental areas, especially those in which a weakened or thinned crust undergoes thermal or mechanical processes associated with rifting and, eventually, oceanic expansion (Allen and Allen, 2013). Depending on the geometry of the previous, inherited fractures and their depth (van Wees et al., 1998), intra-plate rifts may evolve in two ways: (i) along preferred fault directions, in which case subsidence areas are limited by rift shoulders, therefore showing sharp thickness changes in their sedimentary fillings along transects perpendicular to the rift axis; or (ii) rather extending along wide areas showing diffuse borders (Sopeña and Sánchez-Moya, 1997; Liesa et al., 2000). The two stages can be found in the same basins as they evolve from tectonic to thermal subsidence periods (Allen and Allen, 2013). Magmatic processes are common during different stages of rifting evolution. Their extrusive or hypabyssal character depends upon both the volume of magmatic production and the thickness and mechanic stratigraphy of the sedimentary pile. Diapirism is also a non-negligible contribution to deformation during the basinal stages (Vendeville et al., 1995; Alves et al., 2003); salt migration can result both in uplift along major faults related to basin margins (salt walls) and local subsidence in areas surrounding the main diapirs (Fig. 2A). Salt deposition in near coastal environments was common in the western Tethys, because of the latitudinal position near the equator of large regions of Europe and Africa during the Mesozoic (see e.g. Aurell et al., 2007 and references therein). The syn-rift sequences (Permian, Lower Triassic, Upper Triassic, etc.) are characterized by the presence of significant thickness of salt and gypsum (Ziegler, 1982, 1989). Interaction between igneous intrusions and salt diapirism has been also proposed as a mechanism for intra-basinal deformation during the rifting stage (Torres-López et al., 2016). Ductile levels contribute to distribute deformation along larger areas and determine the geometry of the hanging-wall, syn-rift deposits, which can change from roll-over anticlines (reverse drag) to syn-sedimentary synclines (normal drag) at the contact with the basement normal faults bounding the basins or sub-basins (Soto et al., 2007a).

Of particular importance is the relationship between stress axes and the major faults limiting the basin (Fig. 2A), because obliquity between faults and the extension direction can be responsible for transtensional movements thus giving different relationship patterns between faults, the sedimentary infill and the main basin axis (Tron and Brun, 1991). Depocenters location, early deformational structures in syn-rift sediments, overall shape of the basin and (eventually) salt migration can be conditioned by transtension.

Another end-member of intra-plate subsidence is the formation of sedimentary basins associated with fault jogs and bends (Fig. 2A) along strike-slip faults. Although strictly speaking pull-apart and strike-slip-related basins (intra-plate or between different plates) are of relatively small size and linked to very particular conditions of plate movements (Aydin and Nur, 1982; McClay and Dooley, 1995), basin shapes and their sedimentary and magmatic evolution often suggest a certain contribution of this mechanism during, at least, some periods in their tectonic evolution.

The evolution of extensional or transtensional basins can include one or several stages of rifting (Salas and Casas, 1993), characterized by tectonic or thermal subsidence, depending on the processes dominant during the basinal stage, or upon interference with plate or mantle-related processes (Torres-López et al., 2014). The latter can also influence the magnetic properties of rocks (Osete et al., 2011) and hence the magnetic fabrics (Calvín et al., 2018a). As we will discuss later on, AMS can offer a reliable picture of early or intermediate stages of basin evolution, depending on the particular features of the tectonic inversion on each basin that can eventually modify previous, basin-related magnetic fabrics.

2.2. Inversion styles

Inversion of intra-plate basins is linked to changing patterns of plate movements and hence changing stress fields within continental (or oceanic) crust (Ziegler, 1982, 1989; Cloetingh, 1988). Inversion can be either related to stress propagation from the plate boundaries to their inner part (Cloetingh et al., 2002), plate-scale or lithospheric buckling (De Vicente and Vegas, 2009; Fernández-Lozano et al., 2011) or to deep décollements (Guimerà and Alvaro, 1990 and references therein). Modes of inversion depend on different factors (Figs. 2B, 3): i) the dip of major faults limiting the basin, which conditions the frontal or oblique re-activation and inversion, the development of footwall shortcuts and the relative evolution of each wall of the fault (i.e. buttressing or not in the initially downthrown block); ii) the existence of significant detachment levels within the pre-rift sequence; iii) the total shortening during inversion, which can be concentrated on a unique fault or partitioned between different faults with pure reverse or strike-slip movements (De Vicente et al., 2009) and iv) P-T conditions, depending on both the geothermal gradient and the thickness of the sedimentary pile (Mata et al., 2001).

The dip of major faults limiting the basin also influences the relative position of the fault walls with respect to their previous role during extension. That is, the dip of faults defines whether the downthrown block during the extensional stage will become uplifted or remain downthrown during inversion. Steeply-dipping faults can be a catalyst for the relative position of the two blocks to remain unchanged and for folding and thrusting processes to affect the main fault. This one may change its dip sense to finally become a reverse fault. A related process is the buttressing of the syn-rift sequence against steeply-dipping master faults (Fig. 3). Depending on P-T conditions, and favored by burial, this buttressing can lead to cleavage development in the syn-rift sequence. However, pressure-solution cleavage associated with buttressing can also develop at relatively shallow levels. All in all, the particular mechanism of cleavage formation will influence the obtained magnetic fabric, because of the possible re-orientation of phyllosilicates and/or the formation of new mineral phases (Oliva-Urcia et al., 2009).

Finally, the presence of shallow detachment levels is a first-order factor controlling inversion geometry and kinematics, even when basement structures are involved in tectonic inversion (Fig. 3). The possibility of channelizing deformation and transferring displacement to areas located far from the basement thrust fronts makes it easier for extensional basins to form pop-up structures uplifted over the surrounding basement (where syn-rift deposits are much thinner), with or without syn-compressional sedimentation that, in turn, also conditions the final geometry.

3. How to determine the magnetic carriers

3.1. Mineralogies contributing to the AMS

Magnetic mineralogy is a key factor when interpreting magnetic fabrics in sedimentary rocks. Each contributor to the AMS (ferromagnetic, paramagnetic and diamagnetic minerals) must be carefully treated in order to obtain a reliable picture of the bulk magnetic fabric and its significance with respect to the petrofabric. Moreover, it is important to notice that the carriers of the magnetic bulk properties are not necessarily the same minerals that dominate the AMS. After the initial stages of this kind of studies, when AMS analysis was mainly focused on the ferromagnetic *s.l.* fraction (e.g. Fuller, 1969; Graham, 1966), phyllosilicate-rich lithologies (and hence pelites and similar rocks) have been used as ideal markers for magnetic fabrics (e.g. Henry, 1983; Rochette and Vialon, 1984; Borradaile et al., 1986). These rocks usually have low diamagnetic content mostly represented by quartz or calcite minerals and variable ferromagnetic *s.l.* content (i.e., magnetite, hematite, pyrrhotite). In any case, diverse methods for magnetic subfabrics separation allow determining the carriers of the AMS at room temperature (see e.g. Martín Hernández and Ferré, 2007 and references therein). These methods include AMS measurements at low temperature -AMS-LT (e.g. Richter and van der Pluijm, 1994; Lüneburg et al., 1999; Parés and van der Pluijm, 2002a, 2014; Cifelli et al., 2005; Oliva-Urcia et al., 2009; Haerinck et al., 2013; Issachar et al., 2016), measurement of the anisotropy of the anhysteretic remanent magnetization -AARM- (e.g. McCabe et al., 1985; de Wall and Worm, 1993; Borradaile and Jackson, 2004; 2010), the anisotropy of the isothermal remanent magnetization -AIRM- (e.g. de Wall and Worm, 1993; Borradaile and Jackson, 2010) and high field torque measurements -HF-AMS- (e.g. Ferré et al., 2004; Kelso et al., 2002; Martín-Hernández and Hirt, 2001; 2003; 2004; Schmidt et al., 2006; 2007a; 2007b; Haerinck et al., 2013). The applicability of each of these methods is widely discussed below.

It is well stablished that the orientation distribution of all minerals in a specimen is what almost exclusively controls the AMS (i.e., Borradaile and Jackson, 2004 and references therein). Different minerals have different magnetic susceptibility values and anisotropies (Borradaile and Jackson, 2004; 2010 and references therein). Ferromagnetic *s.l.*, paramagnetic and diamagnetic minerals show, respectively, the strongest (positive), lower (positive) and lowest (negative) values of magnetic susceptibility. Pure examples of quartz, calcite and feldspars may have values around -15 10^{-6} SI. Clay minerals, chlorites and micas may range from 100 to 1500 10^{-6} SI, and common iron oxides and sulphides (magnetite, titanomagnetite, titanohematite, hematite and pyrrhotite) show magnetic susceptibilities around 10^{-2} and 10^{0} SI (Borradaile and Jackson, 2010). These minerals are the most typical in sedimentary rocks. Other studies dealing with igneous rocks with abundant presence of olivine and amphiboles, among others, may relate to single crystal studies of those minerals (i.e., Biedermann et al., 2014b; Biedermann et al., 2015).

In particular, in single minerals the crystal structure controls the AMS principal axes orientation. In most of the studied inverted basins (except those whose filling consists of red beds), the most common minerals are phyllosilicates (Table 1), which show a highly oblate ellipsoid of the paramagnetic susceptibility, with the minimum susceptibility direction subparallel to the crystallographic c-axes (Martín-Hernández and Hirt, 2003, and references therein). For the hematite crystal, a widespread mineral in the red beds (Table 1), an intrinsic crystallographic magnetic anisotropy has been described, in which the maximum susceptibility axis is parallel to its basal plane and very weak spin-parallel susceptibility parallelizes the c-axis (Pokorný et al., 2004).

In a few sites from the case studies discussed here, magnetite was also identified (Table 1). The magnetic susceptibility of magnetite can depend on its crystallographic properties (for equidimensional crystals), but most commonly shape and grain size are the main controlling factors. This is because shape anisotropy dominates over the magnetocrystalline one even with low elongation ratios (Winklhofer et al., 1997). Different works (Jackson and Swanson-Hysell, 2012; Calvín et al., 2018b) have shown in remagnetized limestones the dominance of uniaxial magnetite with shape anisotropy. This has some implications since stable single domain (SSD) magnetite with shape anisotropy shows the "inverse fabric" effect (e.g. Potter and Stephenson, 1988) by which the lowest magnetic susceptibility axis is parallel to the long axis of the crystal (the easy direction of magnetization). However, this phenomenon is not so common in sedimentary rocks since SSD grains appear usually together with superparamagnetic (SP) and/or multi-domain (MD) magnetite grains (mainly SP in remagnetized rocks), with higher susceptibility values and lacking the "inverse fabric" effect (e.g. Rochette et al., 1992; Worm and Jackson, 1999; Lanci and Zanella, 2016). Models combining SD –inverse magnetic fabric- and MD –normal magnetic fabric- magnetite reveal intermediate magnetic fabrics, in which its relation with strain is therefore not simple (Ferré et al., 2002). In the studied basins, an interesting application of magnetite-driven fabrics in sedimentary rocks is the contribution of SP magnetite to the AMS, a feature in which remagnetization had a strong influence (Calvín et al., 2018a). In some of the studied basins (Cabuérniga, Cameros, Central High Atlas, Soto et al., 2007b; García-Lasanta et al., 2014, Calvín et al., 2018a), the fabric carried by magnetite indicates the extension direction linked to the basinal stage, and specifically in the Central High Atlas (Imilchil Area), it indicates the stretching at the remagnetization time (Calvín et al., 2018a).

Finally, the presence of pyrrhotite was also observed in some sites (Table 1). Magnetically, pyrrhotite is extremely anisotropic with magnetite-like low-field susceptibility values within the basal plane and values typical of antiferromagnetic material along the crystallographic *c*-axis perpendicular to the basal plane (Schwarz 1975, Martín-Hernández et al., 2008). The AMS of pyrrhotite depends on texture and grain shape (de Wall and Worm, 1993).

3.2. Cookbook for each mixture of minerals

Magnetic mineralogical analyses are essential in every investigation relating AMS to strain. This part of the research has two complementary lines: i) to analyze the magnetic mineralogy itself, traditionally subjecting a few milligrams of powdered sample to various temperatures and magnetic fields (thermomagnetic curves, hysteresis loops, IRM acquisition and back field curves, Fig. 4A, B, C, D), and ii) to obtain more information about the orientation distribution of the different minerals to complement and properly interpret the AMS results in relation to strain (orientation of the minerals measured on the standard specimens). Different magnetic and non-magnetic analyses are accompanying AMS measurements in order to get information about the minerals and their orientation distribution. Complementary, non-magnetic methods require different instrumentation than the standard devices found in a magnetic fabric laboratory: X-Ray goniometry to determine the crystallographic preferred orientation of phyllosilicates or other minerals in relatively small regions (ca. 1 mm^2) (van der Pluijm et al., 1994; de Wall and Worm, 1993; Oliva-Urcia et al., 2009; 2010b; 2012); neutron goniometry to analyze texture by measuring the probable density distribution or pole figure of phyllosilicates (Hansen et al., 2004; Cifelli et al. 2005; 2009); EBSD (electron back scattered diffraction) for measuring the lattice preferred orientation

(LPO) of selected minerals (Prior et al., 1999; Bascou et al., 2005; Hrouda et al., 2009; Oliva-Urcia et al., 2012), which is difficult to perform in marls and siltstones containing phyllosilicates due to the thin section polishing technique. In addition, SEM-EDX observations, XRD and image analyses of dark minerals in thin section (i.e. biotite) are common techniques also used in investigations of AMS related to strain (see e.g. Kodama and Sun, 1990; Lüneburg et al., 1999; Oliva-Urcia et al., 2009). Furthermore, it is possible to model magnetic fabrics from texture data (e.g. Richter et al., 1993; Housen et al., 1993; Hirt et al., 1995; Lüneburg et al., 1999; Chadima et al., 2004; Martín-Hernández et al., 2005; Schmidt et al., 2009; Hastie et al., 2011), providing universal correlations.

The magnetic method to separate subfabrics most easily performed in a magnetic fabric laboratory is the low temperature measurement of the AMS (LT-AMS, Fig. 4E), which requires liquid nitrogen to cool down the samples in a special recipient and a silicon sheet to isolate the coils of the instrument (in the case of KLY3, 4, 3-S, 4-S or superior models, AGICO Inc.; Parés and van der Pluijm, 2002a; 2014; Issachar et al., 2016). This procedure has been largely used in selected sites in the Tethyan extensional basin studies (discussed more extensively below). Once a sample is cooled down, its measurement takes around 30 min (in a KLY3-S, AGICO Inc.). Other magnetic methods easily performed in a paleomagnetic laboratory are the measurement of the anisotropy of the anhysteretic remanence magnetization (AARM; McCabe et al., 1985; Borradaile and Jackson, 2004; 2010), and in some specialized paleomagnetic laboratories, the measurement of AMS at high fields (HF-AMS) in a torque magnetometer (e.g. Martín-Hernández and Hirt, 2004; Martín Hernández and Ferré, 2007; Haerinck et al., 2013; García-Lasanta et al., 2014, 2015). These analyses allow to separate the magnetic subfabrics: the LT-AMS by enhancing the paramagnetic signal of the samples at low temperatures (reliable results are found when LT-AMS/RT-AMS is above 1.5 (e.g. Oliva-Urcia et al., 2016 and references therein) and particularly above 2 in red beds and above 3 in mudstones (Soto et al., 2012) following the Curie-Weiss law, whereas the AARM and the torque magnetometer separate the ferromagnetic fabric of low magnetic coercivity magnetic minerals and high magnetic coercivity minerals with paramagnetic mixture or diamagnetic with paramagnetic mixture (Borradaile and Jackson, 2004, 2010; Martín-Hernández and Hirt, 2004; Schmidt et al., 2007b).

Instruments to perform the magnetic mineralogy analyses are usually found in magnetic fabrics and paleomagnetic laboratories: i) susceptibility vs. temperature curves (k-T curves) in, e.g., KLY3 or KLY4 coupled to CS3 or CS4 ovens (AGICO Inc.); ii) magnetization vs. temperature M-T curves in a Magnetic Measurements Variable Field Translation Balance (MMAVMFTB, Petersen Instruments), in a Micromag 3900 Vibrating Sample Magnetometer (VSM, Princeton Measurement Corp.) or in a Magnetic Properties Measurement System, (MPMS); iii) hysteresis loops in a variable field translation balance, VSM or MPMS; iv) IRM acquisition and backfield curves, as well as thermal demagnetizations of a composite IRM (Lowrie, 1990) in SQUID (cryogenic), spinner (JR5 or 6), by using pulse magnetometers and zero-field ovens.

3.3. Working procedure in inverted basins

The procedure to reveal the main magnetic fabric carriers in the extensional basins of the Tethys has been essentially the same as the standard explained above for other magnetic fabric studies. However, here we present some particular characteristics of these studies.

The information obtained from thermomagnetic curves (hyperbolic decrease of the magnetic susceptibility as temperature increases, and the decay at Curie or Néel temperatures) and ratios of LT/RT bulk magnetic susceptibility indicate that the main AMS carriers in the sampled sediments in these extensional settings are basically paramagnetic minerals, i.e., phyllosilicates (in marine environments; Table 1, Fig. 4A) and ferromagnetic s.l. minerals, i.e. hematite, and phyllosilicates (in continental settings; Table 1, Fig. 4B). Other ferromagnetic carriers different from hematite (i.e., magnetite, iron sulphides) were found in a few sites (e.g. Oliva-Urcia et al., 2013; García-Lasanta et al., 2016). In general, the relationship between the orientation of these ferromagnetic subfabrics and the main RT-AMS orientation is easily established in each case (e.g. Soto et al., 2007b, 2008a; García-Lasanta et al., 2014; Calvín et al., 2018a, 2018b). These ferromagnetic minerals reveal themselves when applying remanence-related analyses (IRM and backfield curves, Fig. 4D).

The observations and results from SEM-EDX analyses were crucial in the Argana Basin to finally discard 28 sites out of 48 (Table 2) since the interchange of magnetic axes found in the basin was clarified when observing thin sections in the SEM-EDX. There, it was possible to identify hematite platelets probably related to a post-extensional fluid mineralization, therefore revealing that the extensional primary fabric had been transformed by a subsequent event. Previously, thermomagnetic curves and LT/RT ratios allowed to infer that paramagnetic minerals and hematite share the same orientation in the studied rocks (Oliva-Urcia et al., 2016). Observations by SEM-EDX were also very useful to visualize and recognize the shape and contacts among minerals at μm-scale in certain basins. In the Organyà and Cabuérniga Basins this technique provided general information about size and qualitative chemical composition of the minerals contributing to the RT-AMS (Oliva-Urcia et al., 2010a; Oliva-Urcia et al., 2013). In the Mauléon Basin, it allowed to check for post-sedimentary transformations, i.e. replacement of pyrite by magnetite, which was not affecting the magnetic fabric, carried here mainly by paramagnetic minerals (Oliva-Urcia et al., 2010c).

The most used way to separate magnetic subfabrics in the Tethyan basins was LT-AMS, since the sampled lithologies were fine-grained (marls, marly limestones, siltstones…), where phyllosilicates (paramagnetic minerals) are abundant (Fig. 4E). In exceptional cases, only one site was analyzed to test the carrier in an anomalously high bulk susceptibility limestone (Soto et al., 2007b). In other studies, systematic analyses were carried out in several selected sites, usually covering the whole range of lithology types and magnetic susceptibility values (Izquierdo-Llavall et al., 2013; García-Lasanta et al., 2015, 2016; Oliva-Urcia et al., 2016 among others). These LT-AMS analyses and the LT/RT ratio of bulk magnetic susceptibility confirm that paramagnetic minerals are the main carriers of the extensional strain in the analyzed rocks in Cameros, Organyà, Mauléon, Cabuérniga and Maestrat Basins (Soto et al., 2007b; 2008a; García-Lasanta et al., 2014; 2016; Oliva-Urcia et al., 2010a; 2010c; Oliva-Urcia et al., 2013). In Triassic red beds, phyllosilicates mimic the hematite fabric in the NW Castillian Branch of the Iberian Range (García-Lasanta et al., 2015), the Triassic Pyrenean basins in the Axial Zone (where extension was recorded in the upper thrust sheets of the antiformal stack: Nogueres Zone; Izquierdo-Llavall et al., 2013) and in some sites of the Argana Basin in the High Atlas (Fig. 4E, Oliva-Urcia et al., 2016).

Analyses to separate the ferromagnetic fabric (generally AARM but also HF-AMS analysis) focused on certain selected sites and allowed to compare the ferromagnetic fabric with the RT-AMS and the LT-AMS; the three of them can be parallel or not. According to the scarce HF-AMS results in the Cameros Basin (García-Lasanta et al., 2014), the ferromagnetic fabric coincides with the RT-AMS (which overlaps with the LT-AMS) for the last extensional stage, and hence this HF-AMS, RT-AMS and LT-AMS overlapping informs about the geological processes acting at the latest stages of the basin evolution. Besides, the coincidence between the AARM and the RT-AMS in most of the limestones sampled in the Central High Atlas suggests a major contribution of magnetite to the bulk magnetic fabric (Calvín et al., 2018a). In this case, the long axis of the magnetic anisotropy ellipsoid has been interpreted to show the extensional direction during authigenic magnetite growth also during basin evolution (Calvín et al., 2018b). In addition, the HF-AMS analyses performed in the Triassic red beds of the NW Castilian Branch Basin of the Iberian Range confirmed that phyllosilicates and hematite (both the saturated and the non saturated part of the signal) share the same orientation distribution (García-Lasanta et al., 2015). These overlappings and the structural observations reveal the primary origin of the RT-AMS. In other cases, when ferromagnetic fabrics are analyzed and they do not overlap RT-AMS/LT-AMS carried by phyllosilicates, they indicate the different timing and strain ellipsoid orientation for the ferromagnetic fabric development respect to the RT-AMS/LT-AMS fabric (Calvín et al., 2018a). This fact is also well known from previous studies from the literature, that do not necessarily relate to inversion of extensional basins. Generally, the ferromagnetic fabric is more randomly oriented than RT-AMS and LT-AMS in the extensional basins and it does not provide compelling information in, for example, the Organyà Basin (Oliva-Urcia et al., 2010a). In other cases, particularly in remagnetized basins, the AARM is not random and its determination has been essential for defining the strain during the basinal stage (Calvín et al., 2018a, 2018b).

Finally, comparison between the magnetic ellipsoids with bedding and other structural elements is basic to interpret the magnetic fabrics. In this sense the clustering degree of the magnetic ellipsoid axes is compared between sites before and after bedding correction. Since remagnetizations are common in sedimentary basins having a thick filling, sometimes it is possible to use it to calculate the paleodip of beds, i.e. to restore the attitude of bedding at the remagnetization time (e.g. Villalaín et al., 2003, 2015; Soto et al., 2008b). To restore the magnetic fabrics according to the paleodip has been useful to understand ferrimagnetic fabrics whose carriers are related to the remagnetization event (Calvín et al., 2018a).

4. AMS patterns

The magnetic fabric can be considered, analogously to finite strain, as a sum of all the processes underwent by the basin (hence its value as a geological marker), including its burial and tectonic history. From a qualitative point of view magnetic fabric could be expressed as:

$$MF=\sum([\text{early diagenesis}]^{a}+[\text{late diagenesis}]^{b}+[\text{early metamorphism}]^{c}+[\text{early inversion processes}]^{d}+[\text{final inversion}]^{e}+[\text{epidiagenesis}]^{f})$$

The exponent (a, b, c, d, e, f) for each process represents its relevance and depends on the mechanisms and specifications involved in each case, especially magnetic mineralogy and the P-T conditions prevailing during that particular period or process, and which are in turn related to the burial history. Not all processes will be able to produce a significant imprint in the magnetic fabric and hence the possibility of defining the extensional stages in basin evolution will depend on the particular conditions of each basin.

4.1. Early magnetic fabrics

The development of magnetic fabrics in sedimentary rocks has been demonstrated to start very early during the deposit of sediments being contemporary with the earliest diagenetic processes, such as compaction and fluids migration (e.g. Kissel et al., 1986; Tarling and Hrouda, 1993; Larrasoaña et al., 2004; Cifelli et al., 2005; Parés et al., 1999; García-Lasanta et al., 2013). The initial shape of the AMS ellipsoid, in sediments deposited in an environment only influenced by the effect of gravitational forces, shows an oblate geometry with the minimum susceptibility axes grouped perpendicular to the bedding plane and magnetic lineation in a radial distribution within the magnetic foliation plane, parallel to bedding (depositional magnetic fabric; Tarling and Hrouda, 1993). When additional hydrodynamic forces (e.g. paleocurrents, tides, etc.) affect the depositional process, the resultant magnetic fabric may be conditioned by them. This influence is translated in a prolate geometry of the AMS ellipsoid with the magnetic lineation oriented in relation with the current direction, and showing different relationship (parallel, perpendicular) depending on its velocity (see e.g. Hamilton and Rees, 1970; Tarling and Hrouda, 1993 for further information).

The depositional mechanism governing the sedimentation of the smallest-size particles ($< 2\ \mu m$) is flocculation (when plates are attached or attracted edge to edge (Meade, 1964), see e.g. García-Lasanta et al., 2016), which is the typical mechanism of deposition in low-energy environments (e.g. alluvial plains or lacustrine areas in continental areas), where sedimentation is only influenced by gravity. In these cases, small-size, platy particles of phyllosilicate grains will accumulate with their [001]-axes (i.e. the minimum susceptibility axes; Martín-Hernández and Hirt, 2003) perpendicular to bedding, and other platy particles (e.g. hematite detrital grains) will lie with their longer axes randomly oriented within the bedding plane.

Due to this early development, magnetic fabrics are able to record, not only the influence of sedimentary conditions, but also the strain pattern controlling the tectonic evolution of the area during sedimentation and early diagenesis (e.g. Kissel et al., 1986; Larrasoaña et al., 2004; Cifelli et al., 2005; references in

Table 1). This capacity is essential to apply AMS as a petrofabric marker in structural studies involving sedimentary rocks, not only in strongly deformed areas (e.g. Graham, 1966; Borradaile and Tarling, 1981; Lowrie and Hirt, 1987; Averbuch et al., 1992; Sagnotti et al., 1999; Borradaile and Jackson, 2004; Parés and Van der Pluijm, 2002a, 2004), but also in contexts where rocks seem to have undergone weak or no deformation (e.g. Kissel et al., 1986; Lowrie and Hirt, 1987; Mattei et al., 1997, 1999; Cifelli et al., 2004, 2005, 2009).

The large variability of tectonic contexts in which AMS has been applied makes possible to establish different relationships between the orientation and shape of the magnetic ellipsoid and the associated strain pattern. Thus, magnetic lineation in compressional-related magnetic fabrics is known to orient parallel to the trend of the compressional structures (i.e. perpendicular to the shortening direction) during the earliest moments of compressional deformation, and parallel to the intersection lineation between bedding and cleavage planes in pervasively deformed areas, to finally become parallel to the stretching direction within the foliation plane (e.g. Borradaile and Jackson, 2004; Parés et al., 1999). Meanwhile, magnetic fabrics associated to an extensional context show their magnetic lineation parallel to the stretching direction and within the bedding dip, therefore perpendicular to the main trend of faults controlling the basin development (e.g. Mattei et al., 1999; Cifelli et al., 2005), whereas their minimum susceptibility axis remains orthogonal to bedding. At grain scale, the phyllosilicates orientation are the carriers of the AMS, with a weak crenulation whose fold axis is parallel to the main stretching direction (Mattei et al., 1999) and with a magnetic lineation related to the spatial distribution of phyllosilicates (in the described case mainly chlorite), lying parallel to the common axis of differently oriented basal planes (Cifelli et al., 2005).

4.2. Total number of data and statistical representation in AMS studies

The general procedure to study extensional-related fabrics in a basin presenting scarce strain markers is to obtain as many AMS sites as possible to cover the whole outcropping area of the basin (from 20 to 95 sites in a basin area of 200 to 600 km^2, Table 2). The sampling is spatially distributed as homogeneously as possible throughout the whole basin, considering a density of sampling of one site for every 2-10 km^2. The number of samples measured per site varying between 9 and 18, to ensure a correct statistical treatment per site. Apart from spreading the sampling of the same lithology throughout the whole basin, one of the goals is to drill, if possible, the finest grain size rocks in order to avoid the effect of paleocurrents or mineralogical artifacts that may hinder the standard interpretation of AMS under extensional conditions (García-Lasanta et al., 2016; Oliva-Urcia et al., 2016).

The next step will consist on classifying the magnetic ellipsoids that result from the standard RT-AMS measurements according to the bulk magnetic susceptibility of samples, their scattering and the orientation variation of the magnetic axes with respect to bedding and/or cleavage. After elucidating the main magnetic fabric carrier(s) and determining magnetic subfabrics, the whole AMS dataset may be properly interpreted in terms of strain acting during extensional basin formation, which has been defined as k_{max} (magnetic lineation) parallel to the main extension direction (Mattei et al., 1997, 1999; Cifelli et al., 2005). Final interpretations will be based on sites in which k_{min} axes dispose perpendicular to bedding.

Subsequent inversion tectonics or fluid circulation events (for example) that may have affected the extensional fabric in certain sites will be singled out thanks to the magnetic mineralogy and the subfabrics separation analyses, and thus discarded from final interpretations about extension directions (i.e., Organyà Basin, Oliva-Urcia et al., 2010a; Pyrenean Axial Zone, Izquierdo-Llavall et al. 2013; Cameros, Maestrat, García-Lasanta et al., 2014; 2016).

4.3. AMS ellipsoids and the deformational style

The key factors intervening in the development of magnetic fabrics related to basin inversion are represented in the double-triangle diagram shown in Fig. 3. The starting point would be extensional or transtensional basins in which the stretching direction is perpendicular or oblique, respectively, to the main border faults. The geometry resulting from inversion is represented by end members (vertexes of the diagram) including (i) buttressing without a relative uplift of the hanging-wall with regard to the foot-wall, (ii) complete inversion with thrusting canalized through a low-strength décollement, (iii) basement-involved uplift without either horizontal displacement or thin-skin thrust sheets. Internal boundaries for the diagram are the limit for foliation development and buttressing structures (that can be coincident or not, depending on the structural level and thus the P-T conditions of deformation). Therefore, most cases of inverted extensional basins should fit between these geometrical end members.

A parallelism can be established between basin/inversion models and AMS patterns (Fig. 5). In order to simplify the final picture of axes directions, we can consider a basinal extension direction parallel to the shortening direction during inversion (which is indeed a situation relatively common or, at least, frequently assumed in many inversion-related structures). Magnetic fabrics resulting from extension would be slightly or totally unchanged in two different situations: when shortening is not significant or when a complete décollement during inversion favors the passive, horizontal displacement of the whole basin and prevents the formation of shortening structures in the hanging wall (i.e. the syn-rift sequence). This means that early fabrics, formed during or shortly after compaction and thus reflecting the extension direction, can be long-lived, provided that no other deformation mechanism is involved during compression.

Maximum modifications of extensional fabrics take place when flattening against the master faults occurs under the adequate P-T conditions or lithology for cleavage formation by re-orientation of phyllosilicates (and/or hematite flakes), or by pressure-solution. These processes are able to change the initial fabric (magnetic foliation becoming parallel to the actual, tectonic foliation and magnetic lineation progressively displacing towards the intersection lineation and then to the stretching lineation as deformation increases), according to models defined by Averbuch et al. (1992), Bakhtari et al. (1998), Parés et al. (1999), and Parés and van der Pluijm (2002b), which described the transition from sedimentary to intermediate fabrics (pencil structure) and to tectonic fabrics. When inversion is related to thin-skin thrust tectonics, each thrust sheet can show its own AMS signature, depending on its position within the thrust sequence and within the frame of the sedimentary basin pre-dating inversion. In a piggy-back thrust sequence, the lower thrust units could reach higher P-T conditions bringing on the development of cleavage and the modification of the previous extensional magnetic fabrics. On the contrary, upper thrust units will potentially preserve inherited fabrics that, although tilted, maintain the necessary information to define the pre-inversion, extension direction.

5. Application to the Western Tethys basins

The Western Tethys provides a broad range of examples of inverted basins, formed under different tectonic contexts and undergoing different types and degrees of inversion (Table 2, Fig. 3). We have centered our review in those belonging to the northern half of the Iberian plate (Pyrenees, Iberian Range and Lusitanian Basin, Fig. 1) and the North African plate (High Atlas, Fig. 1). Both systems formed as a consequence of the extension and convergence between Africa and Iberia (and, secondarily, Europe) in the forelands of the main orogen (Betics-Rif) resulting from the Cenozoic collision between both plates (e.g. De Vicente et al., 2004). The considered extensional basins share a common evolution (with certain particularities) dominated by two rifting cycles, during Late Permian-Triassic and Late Jurassic-Early Cretaceous, respectively, whereas post-rift thermal subsidence governed during Early-Middle Jurassic and Late Cretaceous (Salas et al., 2001) times (Fig. 6).

Basins located in the Iberian Range (central-eastern Iberia) are related either to the Permian-Triassic extension (NW Castilian Branch Basin, Fig. 7A) or the Early Cretaceous stage (Cameros and Maestrat Basins, Figs. 7 B, C), which produced the thickest sedimentary piles within the Iberian plate: up to 8km in the Cameros Basin (Casas-Sainz and Gil-Imaz, 1998; Casas et al., 2009) and up to 4km in the easternmost part of the Maestrat Basin (Martín-Chivelet et al., 2002). Triassic basins were bounded by major faults of lithospheric depth, since magma of asthenospheric origin reached the surface during the Late Triassic (Lago et al. 2005). Thickness changes are very sharp for the Lower Triassic (even more for the strongly subsiding, localized Permian basins; e.g. Sánchez-Moya and Sopeña, 2004) and gentler in the middle-upper part of the series (Sopeña et al., 1988). The obliquity between the main extension direction during the Triassic (close to ENE-WSW, Fig. 8A) and the master faults resulting from Late-Variscan fracturing (Arthaud and Matte, 1977), striking mainly WNW to NW-SE and NE-SW, was responsible for a transtensional pattern during the basinal stage. Triassic syn-rift sequences expand up to Late Triassic times, when thick accumulations of evaporites (Keuper facies) deposited. Active faults during Triassic were partly, extensionally reactivated during the subsequent Late Jurassic-Early Cretaceous rifting stage: Jurassic-Cretaceous basins are controlled by NW-SE and NE-SW-striking deep basement faults (Canérot, 1974; Guiraud and Séguret, 1984; Roca, 1994; Salas and Guimerà, 1997), and locally decoupled from cover faults through the Upper Triassic evaporites.

Inversion styles in the inner part of the plate correspond to classical models of tectonic inversion (Hayward and Graham, 1989; Liesa et al., 2018) conditioned (i) in the lower part of the sequence by the steep dip of normal or strike-slip faults bounding the basins, and (ii) in the upper part of the series by the presence of the Upper Triassic, regional detachment level that allowed for thin-skinned thrusting, especially in the northern and southern basin borders (De Vicente et al., 2009; Guimerà and Alvaro, 1990). The Cameros and Maestrat Basins underwent an inversion conditioned by basement thrusting (Paleozoic and Lower Triassic) with displacement transfer to the Mesozoic cover by means of the Upper Triassic décollement. The thickness of the sedimentary pile and the relationship with master faults determined the occurrence of cleavage during an early inversion stage, widespread in the Cameros basin at depths of more than 3000 m within the synrift sequence, but discontinuous since its occurrence was conditioned by lithological factors (Gil-Imaz et al., 2000). In relation to this cleavage development, changes from an extensional magnetic fabric (with NNE-SSW magnetic lineation, parallel to the regional extension direction) to a compressional one (with magnetic lineation intermediate or parallel, NW-SE, to the intersection lineation) took place. The ferromagnetic fabrics available for this basin (i.e. HF-AMS torque measurements; García-Lasanta et al., 2014) seem to point that this fraction could preserve the extensional fabric even in areas where cleavage post-dating extension was well developed. In the Maestrat Basin, magnetic fabric results allowed to differentiate the influence of two main tectonic processes occurring at the plate-scale during its sedimentary evolution (García-Lasanta et al., 2016): the opening of the Bay of Biscay that triggered the Early Cretaceous rifting in the Iberian domain and the configuration of the western limit of the Tethys Ocean (Fig. 8B).

Pyrenean basins are distributed both along the Europe-Iberia isthmus and the Cantabrian Pyrenees. The Mesozoic basins linked to the Axial Zone that we include in this review (Castejón-Las Paúles Basin in the Nogueres Zone, Organyà Basin and Mauleón Basin; Figs. 7D, E and F, respectively) share some of their features with other Triassic-Cretaceous basins. Moreover, the evolution of the Northern Iberian margin was conditioned from 125 to 83 M.a. by the around 35º counterclockwise rotation of Iberia linked to the opening of the Bay of Biscay (e.g. Van der Voo, 1969; Vissers and Meijer, 2012; Neres et al., 2013). This event influenced the extensional style followed by the Cretaceous Pyrenean basins during their development. Extension started in the region following a transtensive scenario and resulted in the thinning of the continental thrust during an episode of hyper-extension (Jammes et al., 2010), accompanied by partial exhumation of mantle rocks (Lagabrielle and Bodinier, 2008). This scenario is an alternative (but not totally incompatible) with the evolution of a system of pull-apart en-échelon basins during Aptian-Albian times (Choukroune, 1992).

The Pyrenean convergence in the Castejón-Las Paúles Basin led to the detachment of several thrust sheets each showing different degree of deformation. The RT-AMS associated to each thrust sheet allows to establish comparisons in terms of magnetic fabrics changing from cleavage-related to pure extensional or sedimentary fabrics (Fig. 9A, Izquierdo-Llavall et al., 2013). The extensional fabric shows a main NW-SE extensional direction (Fig. 9A, Izquierdo-Llavall et al., 2013) as in López-Gómez et al. (2005) for the Cantabrian-Pyrenean basins. The Early Cretaceous Organyà Basin was transported in the hangingwall of the thrust sheets of the South Pyrenean Central Unit (SPCU, Séguret, 1972), undergoing very little internal deformation during the convergence. Various interpretations are proposed to describe its extensional stage. On one hand, a pure extensional N-S origin is interpreted from the structural analysis in Tavani et al. (2011) or the AMS study in Gong et al. (2009), which also interprets NW-SE magnetic lineation orientations as related to the subsequent compression. On the other hand, AMS investigations, accompanied with brittle structural and rock magnetic analyses, allow separating the AMS data related to the basinal stage from the sites modified due to compression (whose k_{min} axes are not perpendicular to bedding; Oliva-Urcia et al., 2010a). These authors interpret that basinal AMS data define a coexistence of NW-SE and N-S extension directions that occurred during the same tectonic event, associated with a regional extension (far-field) direction oblique to the main E-W Pyrenean faults controlling sedimentation (Fig. 9B).

A very particular context surrounds the Mauléon Basin (Fig. 7F), located along the North-Pyrenean fault. It is a strongly subsiding basin filled with up to 1500m-thick of black marls and interpreted as resulting from pull-apart mechanisms (Debroas, 1990) coeval to the hyper-extension episode (Jammes et al., 2010) along the Iberia-Europe margin. The basin formed under strong geothermal gradients and accommodated strike-slip movements related to the opening of the Bay of Biscay and the rotation of Iberia during the Aptian-Albian. During the Pyrenean compression, buttressing of the Mauléon Basin infill led to cleavage development across syn-rift units and produced the re-arrangement of its early magnetic fabrics close to the main basin-bounding faults, whereas extensional magnetic fabrics remained in few sites depending on their position with respect to basin margin faults and heterogeneous deformation areas (Fig. 9C, Oliva-Urcia et al., 2010c).

The Cantabrian basins record a complex sedimentary history since the Triassic and up to the Early Cretaceous, characterized with high subsidence rates, comparable to those obtained in the Cameros or the Organyà Basins. An intra-Cretaceous uplift stage (Soto et al., 2011) invokes a contribution of strike-slip tectonics, probably linked to the sinistral movement of Iberia with respect to Europe (Soto et al., 2011), but the record of this movement was probably obliterated during wholesale inversion of the basins, in which the main WNW-ESE faults, oblique to the Cantabrian margin, were re-activated as reverse-dextral faults (Oviedo, Saltacaballos,…). In this area, the change of magnetic fabrics along the stratigraphic sequence (as also occurring in the Cameros Basin, Soto et al., 2008a; García-Lasanta et al., 2014) indicates changes in the boundary conditions of the margins of the Iberian plate during Mesozoic times (Fig. 8C). Limited cleavage development associated with buttressing and inversion points to a N-S shortening during the Cenozoic (Fig. 7G; Table 2), consistent with the orientation of magnetic fabrics (E-W vertical magnetic foliation and E-W horizontal lineation, Fig. 9D; Soto et al., 2007b; Oliva-Urcia et al., 2013). Compression-related magnetic fabrics extend along a portion of the stratigraphic sequence that is slightly wider than the portion affected by cleavage. This distribution evidences that extensional magnetic fabrics can be only interpreted when there is a minimum separation (in the vertical or the horizontal) to the cleavage front and k_{min} remains perpendicular to bedding and does not show a girdle (either incipient or well-developed) distribution (Fig. 9D; Oliva-Urcia et al., 2013).

Magnetic fabrics in the western coast of Iberia do not reflect a simple history, as could be thought from a first approach at the structure. Up to four rifting phases have been recognized in the Lusitanian Basin, being the first (Late Triassic-Hettangian) and the third (Late Jurassic) studied by means of AMS analyses (Soto et al., 2012 and references therein). This study determined a change in extension directions with time in the passive margin, without influence of inversion structures, from almost radial with a subtle main NW-SE extension direction in the Late Triassic to NE-SW extension direction in the Late Jurassic. Both orientations are oblique to the broadly N-S (in present-day coordinates) extensional structure of the continental margin but consistent with the beginning of oceanic extension and contrasting with the rifting evolution in the Iberian Range. The Late Jurassic NE-SW extension direction was interpreted in relation to secondary processes linked to the regional E-W stretching and the Atlantic Ocean spreading (Fig. 10A, Soto et al., 2012).

The basinal evolution of the Triassic Argana Basin, in the Atlantic Moroccan coast, shares some common features with the western coast of Iberia during the Mesozoic. In both cases, the reactivation of Paleozoic structures oriented N-S and NNE-SSW as transtensional to pure extensional controlled the Triassic basinal development according to a NW-SE orientation. The process led to thickness variations in the Triassic sequence between 1 km in the offshore area to 3 km in Argana Basin (Baudon et al., 2012; Fig. 10B). Weak inversion is observed in this basin, since the main extensional faults were not re-activated during shortening (Laville et al., 1977). Interestingly, in this case, the magnetic fabrics analyses allowed describing the mean WNW-ESE extensional direction for 20 sites (out of the total 48) that corresponds to the far field extension driven by rifting (and later oceanic spreading) in the Atlantic margin (Fig. 10B, Oliva-Urcia et al., 2016).

The other Mesozoic basins located along the Moroccan High Atlas Range display different histories depending on their position in relation to the main faults and axis of the basin/Range. The evolution of the Middle Jurassic to the Early Cretaceous basins (dominated by red beds sequences, up to 500m in Aït-Attab Basin and 875m in Ouauitzaght Basin Figs. 7J, K) are controlled, as in the other Mesozoic basins, by the reactivation of Variscan faults, although the tectonic regime during sedimentation is not yet clear (Moussaid et al., 2013 and references therein). The RT-AMS analyses lead to interpret a compressional-related origin for the Aït-Attab Basin and a transtensional-related origin associated with directional movements on the major faults having Atlasic directions for the Ouauitzaght Basin (Figs. 10C, D; Moussaid et al., 2013). The contribution of a strike-slip component is clearer in the case of the Ouaouitzaght Basin, according to the basin shape and its inversion features.

The sedimentary sequence in the Central High Atlas Basin (Imichil area Fig. 7L) is characterized by a thick sedimentary cover (up to 5 km in the depocentres) of Jurassic rocks affected by a remagnetization at ca 100 Ma (Torres-López et al., 2014, 2016; Calvín et al., 2017). Relatively weak deformation is associated to tectonic inversion, which took place through a thick Triassic detachment level and resulted in the decoupling of the basement and the Jurassic cover (Calvín et al., 2017 and references therein). The principal structures observed in the area are thrusts at the northern and southern margins and tightening of previously developed folded structures in its central part. Cleavage developed in favorable lithologies and positions within the stratigraphic pile (Calvín et al., 2017). The remagnetization postdates magmatic and salt-tectonics-related events that contributed significantly to the early structuring of the central part of the Atlas Range before the onset of compression, and clearly predates cleavage formation (Frizon de Lamotte et al., 2009; Vergés et al., 2014; Calvín et al., 2017). Magnetic fabrics reflect both the NW-SE extension direction during the basinal stage and the compression perpendicular to the basin axis during the Cenozoic (defining a NE-SW magnetic lineation). Magnetic fabrics are strongly conditioned by lithology (marls tend to register compressional fabrics, whereas limestones record extensional ones) and structures at the outcrop scale (compressional cleavage, also related to lithology). As mentioned in the previous section in this review about magnetic mineralogies, this distinction is also related to the origin (para- or magnetite-related ferromagnetic) of the magnetic fabrics (Calvín et al., 2018a).

6. Discussion

The above exposed studies of different basinal and inversion styles provide robust patterns of AMS-tectonics relationships that can be extrapolated to the study of other basins worldwide. In this section we discuss the range of applicability and limitations to this technique.

On the side of magnetic mineralogy, both ferro- and paramagnetic fabrics can give information about the extensional stage and the subsequent compression. Classically, paramagnetic minerals, namely phyllosilicates, have been considered a good marker for deformation. This is clear in the case of shortening, because the axes of folds coincide with the zone axis for planar grains within a deformed volume of rock, and hence with the magnetic lineation (Borradaile and Jackson, 2010; Anastasio et al., 2015). The sensitivity of AMS analyses respect to classical strain analyses is higher as seen in the weakly deformed Appalachian sandstones (Burmeister et al., 2009). Under extension, the coincidence between the stretching direction and the magnetic lineation (e.g. Mattei et al., 1997, 1999; Cifelli et al., 2005; García-Lasanta et al., 2014, 2015, 2016) must be explained by the preferred, although weaker, orientation of initially parallel grains in a similar way. The recognition of one or other basinal processes depends on their relative importance, the p-T conditions (and thus burial/exhumation history) and the particular magnetic mineralogy intervening in each process.

An important distinction must be done between magnetite- and hematite-driven ferromagnetic fabrics, since the behavior of primary hematite reproduces almost perfectly the fabric of paramagnetic minerals (i.e. phyllosilicates) due to their magnetocrystalline anisotropy. Magnetite-driven fabric also shows a strong dependency on the state of magnetite due to its shape and distribution anisotropy. Superparamagnetic grains grown during remagnetization stages provide a record of strain precisely during this stage (Calvín et al., 2018a) and therefore give new possibilities for dating magnetic fabrics. In general, no inverse fabrics were found in the different basins presented in this work, which can be measured by the anisotropy of the remanence. Paradoxically, the more anomalous results were found linked to hematite-bearing rocks (red beds) and not to magnetite-bearing rocks. Axes switching occurs probably linked to precipitation of hematite during diagenesis forming aggregates able to disturb the bulk magnetic fabric (Fig. 10B, Oliva-Urcia et al., 2016). The fact that these anomalies occur in sandstones and not in lutites points to secondary fluid circulation as the responsible for this phenomenon, that could be possibly avoided by applying harder criteria in the selection of sampling sites.

Timing of development (also called fixation, blocking, etc.; see García-Lasanta et al., 2013 for a discussion) of the magnetic fabric is also a major issue in interpreting AMS in sedimentary basins. From the examples presented, it can be inferred that magnetic fabric is a dynamic marker that can change according to the P-T conditions and deformation of rocks during their history. The first stages, in which deposition takes place, are of crucial importance (García-Lasanta et al., 2013) in the arrangement of sedimentary particles, and hence the possibility of recording extensional, syn-sedimentary features. However, a stage of "blocking" of the magnetic fabric cannot be recognized because under new conditions, provided that they are able to change the orientation of phyllosilicates or to create new ferromagnetic phases according to the prevailing strain field, magnetic fabrics can also change.

Recognizing each of the phases that build the total magnetic fabric is an important task that can be accomplished by complementary techniques, either magnetic (determination of ferromagnetic subfabrics, AARM and AIRM, or enhanced, LT paramagnetic subfabrics) or non-magnetic (e.g. thin sections under the petrological microscope, electronic microscopy, SEM-EDX observations, X-Ray goniometry, neutron goniometry, electron back scattered diffraction, XRD and image analyses, or even AMS modeling).

A major factor often oversimplified in tectonic inversion studies is the angular relationship (obliquity or parallelism) between the extension and compression directions ("translated" to shortening and stretching directions when considering rock volumes and AMS or finite strain analysis) during the basinal and inversion stages, respectively (see discussion in its application to the Cameros Basin, e.g. in Casas-Sainz and Gil-Imaz, 1994). As previously mentioned (Fig. 5 and related paragraphs), coaxiality can contribute to enhance the resulting magnetic fabric, provided that the minimum horizontal stress axis coincides in both stages. Although we have also considered end-members of strain directions in the classification of magnetic fabrics and their possible evolution (Fig. 5), intermediate positions are probably the most common situations. However, the strong constraint imposed by fault reactivation at the basin margins can also deviate the remote (or "regional") stress directions, more easily during compression (see e.g. Casas et al., 1992; Liesa and Simón, 2009; Simón and Liesa, 2011), making them perpendicular to the reverse faults (e.g. Oliva et al., 2010a). In any case, zonation of strain axes obtained from AMS can give a portrait of changes resulting alternatively (or both) from (i) the occurrence of secondary faults and interference by local structures and associated deviations and from (ii) changes at the regional scale (remote stress), controlled, for example, by rifting linked to different mechanisms or different, active plate margins (Figs. 10A, 8B, Soto et al., 2012; García-Lasanta et al., 2016). Unexpected results in terms of extension direction can give the clues for defining, in some cases, the large-scale evolution of sedimentary basins (Soto et al., 2008a). Cautiously deciphering the directional features of AMS in relation to the master faults is necessary to correctly interpret basin evolution.

The examples shown provide a picture of the Mesozoic-Cenozoic evolution of the westernmost part of Africa and Eurasia from which some insights into the geodynamics of the area can be obtained. Triassic rifting was strongly controlled by basement faults probably reaching the base of the lithosphere, inherited from Late-Variscan fracturing (Arthaud and Matte, 1977; García-Lasanta et al., 2015 and references therein, Fig. 8A). Extension was controlled by N-S faulting along the future passive margin related to the opening of the Atlantic Ocean (Mattauer et al, 1977; Rasmussen et al., 1998) only in the westernmost margin of Iberia-Africa. Evolution of Cretaceous Pyrenean basins (Basque-Cantabrian, North-Pyrenean and South-Pyrenean), including early inversion stages, support a period of strike-slip or transtensional deformation rather than an extension linked to a frontal divergence between Iberia and Europe. Although hyperextension is the widely accepted model at this moment to explain the opening of the Pyrenean realm during the Mesozoic and the exposures of mantle rocks at surface (Masini et al., 2014; Tugend et al., 2014), the oblique extension directions obtained from AMS (Fig. 9B, point to a significant component of oblique extension consistent with a transtensional movement of Iberia at this time (what agrees, on the other hand, with other models based on magnetic anomalies in the ocean floor, where transpression is also reflected (Rosenbaum et al., 2002; Sibuet et al., 2004).

Magnetic fabrics show a strong influence of the early stages in basin evolution; therefore, characterizing shortening directions from AMS is not straightforward. The degree of deformation inferred from structural indicators is consistent both with the above-mentioned factors particular of each basin and with their position within the plate. A deformation gradient can be established from Pyrenean basins (undergoing stronger deformation during compression, as corresponding to a continental subduction plate-boundary) to Atlasic and Iberian basins (located in equivalent positions with respect to plate margins), that grade from total to partial or almost null inversion (Fig. 3), and finally to Atlantic-bounded basins that occupy marginal areas in the compressional Eurasia-Iberia-Africa convergence system.

7. Conclusions

Anisotropy of Magnetic Susceptibility has become a first-order tool for the study of the evolution of inverted sedimentary basins. The magnetic fabric of pelitic rocks records the extensional and the inversion histories, providing a composite picture that must be deciphered by separating sub-fabrics carried by different minerals, and the aid of geological indicators, at the macro- (master faults limiting the basin), meso- (cleavage and faults at the outcrop scale) and micro- (interaction between grains and pressure-solution surfaces) scales. Consistent magnetic fabrics are carried in general by paramagnetic (mainly phyllosilicates) and ferromagnetic minerals. Among the second group, hematite is a reliable carrier to obtain direct information about extensional stage although some tests must be done to guarantee its primary origin in relation to sedimentation or early diagenesis (or the prevalence of these stages in relation to other subsequent processes in the imprint to the magnetic fabric). The selection of fine-grained lithologies where post-depositional fluid circulation is limited can help to constrain this issue. Other ferromagnetic carriers such as pyrrhotite and magnetite can give valuable information about the extensional stage, especially in basins where there is a remagnetization associated with the basinal stage, triggered by chemical or thermal processes. Sub-fabric separation by different methods and cross-correlation between present-day dips, paleodips and orientation of AMS axes can help in dating the different tectonic stages associated with subfabrics. Magnetic fabrics, and hence mineral grain orientation can be explained by plastic deformation of beds that determines the preferred orientation of platy grains. In the case of magnetite-carried fabrics, oxidation of previous, iron-rich paramagnetic grains (pyrite and other iron sulphides) probably plays a major role. Both the remote stress field determined by deformation at the plate margins and the local stress resulting from the interaction with major faults at the basin margin (or secondary faults within the basin) influence the deformation of the rock volume and hence the final magnetic fabric. A minimum number of even-distributed sites is necessary to determine the significance of each of the two variables.

Determining the contribution of basinal (extensional) and compressional (inversion) deformation to the total magnetic fabric is a major issue in understanding of the internal deformation underwent by the basin fill. This also depends on the particular conditions of each basin, including the mechanical stratigraphy of the pre-rift sequence (here the presence/absence of detachment levels plays a major role), the geometry of major faults, its P-T evolution and its location with respect to the main tectonic traits within the plate. Considering the different types of basins, in first instance the perpendicularity or obliquity to the major faults gives clues for interpreting transtensional components and hence the prevalence of crustal- or lithospheric-scale fracture zones vs. newly formed faults. Fixation or evolution of the magnetic fabrics along time mainly depends on the possibility of modifying the orientation of phyllosilicates during the inversion stage (under relatively high temperature gradients) or of oxidation/crystallization of ferromagnetic phases.

The results presented, including a number of basins within the Iberian and North African plates, show a strong imprint of Late-Variscan or Early Mesozoic faults, resulting in transtension during the first rifting stages (Triassic) in the inner part of the plates, and extension orthogonal to the main faults near the Atlantic margin of Africa and Iberia. This situation evolved towards NE-SW (Pyrenean) and NW-SE (Tethyan, including Atlasic extension) during the Jurassic and Early Cretaceous. Inversion took place in a variety of tectonic environments, above and below the cleavage front, with (i) buttressing, tight folding and cleavage development, thus deflecting the original extensional magnetic fabric; (ii) inversion associated with transport in the hangingwall of thrust sheets, either unique or superimposed, in which the presence of low-strength levels favored preservation of structures; (iii) weak inversion preserving the original structures and magnetic fabrics.

As a summary, the application of AMS (and subfabric separation) analyses in inverted sedimentary basins has been fundamental for:

- Covering extensive areas in a relatively short time of basin outcrops where strain markers are absent or scarce in order to determine extensional strain (in basins formed under such conditions), once the relationship between magnetic fabrics and microstructures has been established. Even where conventional geological markers are missing, we can define the deformation ellipsoid, related with either of the geological processes underwent by the sedimentary basin.
- Discerning a possible coaxiality or non-coaxiality of extensional and compressional strains, an issue that often constitutes the hobbyhorse in drawing cross-sections of inverted basins, and a fundamental step for defining the transport direction for both extension and compression and correct basin reconstruction.
- Determining the extensional strain variations through time and/or space or a zonation according to the prevalence of different plate-margin processes (in our case, applied to the Basque-Cantabrian, Cameros, Maestrat, Lusitanian, and Iberian Castillian branch basins).
- Qualitatively determining the strain threshold necessary for a compressional fabric to be present (defined in the Cabuérniga, and the Aït Attab remagnetized Central High Atlas basins). This also allows for zoning inverted sedimentary basins in relation to older extensional structures and for establishing a hierarchy of structures depending on their contribution to the final basin structuring.

- Determining the zonation or the partition of the compressional deformation after the extensional stage (Mauléon and Organyà basins), that can give clues about the existence of possible strike-slip components derived from the external field or interference with intra-basinal structures.

Acknowledgements

The authors are grateful to Fabio Speranza and two anonymous referees for their thorough revisions of the manuscript. We also acknowledge the use of Servicio de Apoyo a la Investigación-SAI, Universidad de Zaragoza. This study has been financed by the research projects CGL2009-08969 (UZ), CGL2016-77560-C2-1-P and CGL2016-77560-C2-2-P of the MICINN (Spanish Ministry of Science and Innovation).

References

Aydin, A., Nur, A., 1982. Evolution of pull-apart basins and their scale independence. Tectonics 1(1), 91-105.

Allen, P.A., Allen, J.R., 2013. Basin analysis: principles and application to petroleum play assessment. John Wiley & Sons.

Alves, T.M., Manuppella, G., Gawthorpe, R.L., Hunt, D.W., Monteiro, J.H., 2003. The depositional evolution of diapir-and fault-bounded rift basins: examples from the Lusitanian Basin of West Iberia. Sedimentary Geology 162 (3-4), 273-303.

Anastasio, D., Parés, J.M., Kodama, K.P., Troy, J., Pueyo, E.L., 2015. Anisotropy of magnetic susceptibility (AMS) records synsedimentary deformation kinematics at Pico del Aguila Anticline, Pyrenees, Spain. Special Publication - Geological Society of London 425, 1, 129-144, 16.

Antolín-Tomás, B., Román-Berdiel, T., Casas-Sainz, A., Gil-Peña, I., Oliva, B., Soto, R., 2009. Structural and magnetic fabric study of the Marimanha granite (axial zone of the Pyrenees). International Journal of Earth Sciences 98(2), 427–441.

Aranguren, A., 1997. Magnetic fabric and 3D geometry of the Hombreiro-Sta Eulalia pluton: implications for the Variscan structures of eastern Galicia, NW Spain. Tectonophysics 273, 329-344.

Arthaud, F., Matte, P., 1977. Late Paleozoic strike-slip faulting in southern Europe and northern Africa: Result of a right-lateral shear zone between the Appalachians and the Urals. Geological Society of America Bulletin 88(9), 1305-1320.

Aubourg, C., Rochette, P., Stephan, J.F., Popoff, M., Chabert-Pelline, C., 1999. The magnetic fabric of weakly deformed Late Jurassic shales from the southern subalpines Ranges (French Alps. evidence for SW-directed tectonic transport direction. Tectonophysics 307, 15-31.

Auréjac, J.B., Gleizes, G., Diot, H., Bouchez, J.L., 2004. Le complexe granitique de Quérigut (Pyrénées, France) ré-examiné par la technique de l'ASM: un pluton syntectonique de la transpression dextre hercynienne. Bulletin de la Société Géologique de France 175(2), 157–174.

Aurell, M., Bádenas, B., Casas, A.M., Salas, R., 2007. Peritidal carbonate-evaporite sedimentation coeval to normal fault segmentation during the Triassic-Jurassic transition, Iberian Range. In: Nichols, G.J., Paola, C. & Williams, E.A. (eds) Sedimentary processes, environments and basins – a tribute to Peter Friend. Int. Assoc. Sedim., Spec. Pub. 38, 219-240.

Aydin, A., Nur, A., 1982. Evolution of pull-apart basins and their scale independence. *Tectonics 1*(1), 91-105.

Averbuch, O., Frizon de Lamotte, D., Kissel, C. 1992. Magnetic fabric as a structural indicator of the deformation path within a fold-thrust structure: a test case from the Corbières (NE Pyrenees, France). Journal of Structural Geology 14, 461-474.

Bakhtari, H.R., de Lamotte, D.F., Aubourg, C., Hassanzadeh, J., 1998. Magnetic fabrics of tertiary sandstones from the Arc of Fars (Eastern Zagros, Iran). Tectonophysics 284(3-4), 299-316.

Bascou, J., Camps, P., Dautria, J.M., 2005. Magnetic versus crystallographic fabrics in a basaltic lava flow. Journal of Volcanology and Geothermal Research 145(1), 119-135.

Baudon, C., Redfern, J., Van Den Driessche, J., 2012. Permo-Triassic structuralevolution of the Argana Valley, impact of the Atlantic rifting in the High Atlas,Morocco. Journal of African Earth Sciences 65, 91-104.

Biedermann, A.R., Bender Koch, C., Lorenz, W.E.A., Hirt, A.M., 2014a. Low-temperature magnetic anisotropy in micas and chlorite. Tectonophysics 629, 63-74.

Biedermann, A.R., Pettke, T., Reusser, E., Hirt, A.M., 2014b. Anisotropy of magnetic susceptibility in natural olivine single crystals. Geochemistry Geophysics Geosystems 15(7), 3051-3065.

Biedermann, A.R., Bender Koch, C., Pettke, T., Hirt, A.M., 2015. Magnetic anisotropy in natural amphibole crystals. American Mineralogist 100(8-9), 1940-1951.

Biedermann, A.R., Kunze, K., Hirt, A.M., 2018. Interpreting magnetic fabrics in amphibole-bearing rocks. Tectonophysics 722, 566-576.

Bilardello, D., 2016. Magnetic Anisotropy: Theory, Instrumentation, and Techniques. Reference Module in Earth Systems and environmental Sciences.

Borradaile, G.J., 1987. Anisotropy of magnetic susceptibility; rock composition versus strain. Tectonophysics 138, 2-4, 327-329.

Borradaile, G.J., 1988. Magnetic susceptibility, petrofabrics and strain. Tectonophysics 156, 1–20.

Borradaile, G.J., 1991. Correlation of strain with anisotropy of magnetic susceptibility (AMS). Pure and Applied Geophysics 135, 1, 15-29.

Borradaile, G.J., Tarling, D.H., 1981. The influence of deformation mechanics on magnetic fabrics in weakly deformed rocks. Tectonophysics 77, 151-168.

Borradaile, G., Mothersill, J., Tarling, D., Alford, C. 1986. Sources of magnetic susceptibility in a slate. Earth and Planetary Science Letters 76 (3-4) 336-340.

Borradaile, G.J., Henry, B., 1997. Tectonic applications of magnetic susceptibility and its anisotropy. Earth Sci. Rev. 42, 49–93.

Borradaile, G.J., Jackson, M., 2004. Anisotropy of magnetic susceptibility (AMS); magnetic petrofabrics of deformed rocks. Geol. Soc. Spec. Publ. 238, 299–360.

Borradaile, G.J., Jackson, M., 2010. Structural geology, petrofabrics and magnetic fabrics (ASM, AARM, AIRM). Journal of Structural Geology 32, 1519-1551.

Bouchez, J.L., 1997. Granite is never isotropic: an introduction to AMS studies of granitic rocks. In: Bouchez J.L., Hutton D.H.W., Stephens W.E. (eds) Granite: from segregation of melt to emplacement fabrics. Kluwer, Dordrecht, 95-112.

Bouchez, J.L., 2000. Magnetic susceptibility anisotropy and fabrics in granites. Comptes Rendus de l'Académie des Sciences Series IIA Earth and Planetary Science 330 (1), 1–14.

Burmeister, K.C., Harrinson, M.J., Marshak, S., Ferre, E.C., Bannister, R.A., Kodama, K.P., 2009. Comparison of Fry strain ellipse and AMS ellipsoid trends to tectonic fabric trends in very low-strain sandstone of the Appalachian fold-thrust belt. Journal of Structural Geology 31, 9, 1028-1038.

Brun, J.-P., Nalpas, T., 1996. Graben inversion in nature and experiments. Tectonics 15, 3, 677-687.

Calvín, P., Casas-Sainz, A.M., Villalain, J.J., Moussaid, B., 2017. Diachronous folding and cleavage in an intraplate setting (Central High Atlas, Morocco) determined through the study of remagnetizations. Journal of Structural Geology 97, 144-160.

Calvín, P., Villalaín, J.J., Casas-Sainz, A.M., 2018a. The carriers of AMS in remagnetized carbonates. Insights for remagnetization mechanism and basin evolution. Physics of the Earth Planetary Interiors, 282, 1-20.

Calvín P., Villalaín, J.J., Casas-Sainz, A.M. 2018b. Anisotropic magnetite growth in remagnetized limestones. Tectonic constraints and implications of the basin history. Geology. doi: 10.1130/G45158.1

Canérot, J., 1974. Recherches géologiques aux confins des chaînes ibérique et catalane (Espagne) Doctoral dissertation, Laboratoire de géologie de l'Université Paul Sabatier.

Cañón-Tapia, E., Mendoza-Borunda, R., 2014. Magnetic petrofabric of igneous rocks: Lessons from pyroclastic density current deposits and obsidians. Journal of Volcanology and Geothermal Research 289, 151-169.

Casas, A.M., Simon, J.L., Serón, F.J., 1992. Stress deflection in a tectonic compressional field: a model for the Northwestern Iberian Chain, Spain. Journal of Geophysical Research: Solid Earth 97(B5), 7183-7192.

Casas, A.M., Villalaín, J.J., Soto, R., Gil-Imaz, A., Del Río, P., Fernández, G., 2009. Multidisciplinary approach to an extensional syncline model for the Mesozoic Cameros Basin (N Spain). Tectonophysics 470, 3-20.

Casas-Sainz, A.M., Gil-Imaz, A., 1994. Evolución tectonosedimentaria de una cuenca extensional intraplaca: la cuenca finijurásica-eocretácica de los Cameros (La Rioja-Soria): Discusión. Revista de la Sociedad Geológica de España 7(3-4), 337-347.

Casas-Sainz, A.M., Gil-Imaz, A., 1998. Extensional subsidence, contractional folding and thrust inversion of the Eastern Cameros Massif, northern Spain. Geologische Rundschau 86, 802-818.

Casas-Sainz, A.M., Román-Berdiel, T., Oliva-Urcia, B., García-Lasanta, C., Villalaín, J.J., Aldega, L., Corrado, S., Caricchi, C., Invernizzi, C., Osácar, M.C., 2017. Multidisciplinary approach to constrain kinematics of fault zones at shallow depths: a case study from the Cameros–Demanda thrust (North Spain). International Journal of Earth Sciences 106, 1023-1055.

Casas-Sainz, A.M., Gil-Imaz, A., Simón, J.L., Izquierdo-Llavall, E., Aldega, L., Román-Berdiel, T., Osácar, M.C., Pueyo-Anchuela, Ó., Ansón, M., García-Lasanta, C., Corrado, S., Invernizzi, C., Caricchi, C., 2018. Strain indicators and magnetic fabric in intraplate fault zones: Case study of Daroca thrust, Iberian Chain, Sapin. Tectonophysics, doi: 10.1016/j.tecto.2018.02.013

Chadima, M., Hansen, A., Hirt, A.M., Hrouda, F., Siemens, H., 2004. Phyllosilicate preferred orientation as a control of magnetic fabric; evidence from neutron texture goniometry and low and high-field magnetic anisotropy (SE Rhenohercynian Zone of Bohemian Massif). Geological Society Special Publication 238, 361-380.

Choukroune, P., 1992. Tectonic evolution of the Pyrenees. Université des Sciences et Techniques du Languedoc / Elf.- ERAP. Boussens.

Cifelli F., Mattei M., Hirt A.M., Günther A., 2004. The origin of tectonic fabrics in “undeformed” clays: The early stages of deformation in extensional sedimentary basins. Geophysical Research Letters 31, L09604.

Cifelli, F., Mattei, M., Chadima, M., Hirt, A.M., Hansen, A., 2005. The origin of tectonic lineation in extensional basins: combined neutron texture and magnetic analyses on “undeformed” clays. Earth and Planetary Science Letters 235, 62-78.

Cifelli, F., Mattei, M., Chadima, M., Lenser, S., Hirt, A.M., 2009. The magnetic fabric in “undeformed clays”: AMS and neutron texture analyses from the Rif Range (Morocco). Tectonophysics 466(1), 79-88.

Cloetingh, S., 1988. In: New perspectives in basin analysis (pp. 205-230). Springer New York.

Cloetingh, S., Burov, E., Beekman, F., Andeweg, B., Andriessen, P.A.M., Garcia-Castellanos, D., De Vicente, G., Vegas, R., 2002. Lithospheric folding in Iberia. Tectonics 21 (5), 1041–1067.

De Graciansky, P.C., Dardeau, G., Lemoine, M., Tricart, P., 1989. The inverted margin of the French Alps and foreland basin inversion. Geological Society, London, Special Publications 44 (1), 87-104.

De Vicente, G., Vegas, R., 2009. Large-scale distributed deformation controlled topography along the western Africa-Eurasia limit: Tectonic constraints 474: 124-143.

De Vicente, G., Vegas, R., Casas, A., 2004. Estructura y evolución alpina de la Cadena Ibérica. In: J.A. Vera (ed.) Geología de España. S.G.E.-I.G.M.E., Madrid, 525-526.

De Vicente, G., Vegas, R., Muñoz-Martín, A., Van Wess, J.D., Casas-Sáinz, A., Sopeña, A., Sánchez-

Moya, Y., Arche, A., López-Gómez, J., Olaiz, A., Fernández-Lozano, J., 2009. Oblique strain partitioning and transpression on an inverted rift: The Castilian Branch. Tectonophysics 470, 224–242.

de Wall, H., Worm, H.-U., 1993. Field dependence of magnetic anisotropy in pyrrhotite: effects of texture and grain shape. Physics of the Earth and Planetary Interiors 76, 137-149.

Debroas, E.J., 1990. Le flysch noir albo-cenomanien témoin de la structuration albienne a senonienne de la Zone nord-pyrénéenne en Bigorre (Hautes-Pyrénées, France). Bulletin de la Société Géologique de France 6, 2, 273-285.

Fernández Lozano, J., Sokoutis, D., Willingshofer, E., Cloetingh, S., De Vicente, G., 2011. Cenozoic deformation of Iberia; a model for intraplate mountain building and basin development based on analogue modeling. Tectonics 30, 1, TC1001.

Ferré, E.C., 2002. Theoretical models of intermediate and inverse AMS fabrics. Geophysical Research Letters 29(7), 31-1.

Ferré, E.C., Martin-Hernandez, F., Teyssier, C., Jackson, M., 2004. Paramagnetic and ferromagnetic AMS in migmatites: Measurements in high and low fields and kinematic implications. Geophysical Journal International 157, 1119-1129.

Frizon de Lamotte, D., Leturmy, P., Missenard, Y., Khomsi, S., Ruiz, G., Saddiqi, O., Guillocheau, F., Michard, A., 2009. Mesozoic and Cenozoic vertical movements in the Atlas system (Algeria, Morocco, Tunisia); an overview. Tectonophysics 475, 9-28.

Fuller, M. 1969. Magnetic orientation of borehole cores. Geophysics 34, 772-774.

García-Lasanta, C., Oliva-Urcia, B., Román-Berdiel, T., Casas, A.M., Pérez-Lorente, F., 2013. Development of magnetic fabrics in sedimentary rocks: insights from early compactional structures (ECS). Geophysical Journal International 194 (1), 182-199.

García-Lasanta, C., Oliva-Urcia, B., Román-Berdiel, T., Casas-Sainz, A., Hirt, A.M., 2014. Undestanding the Mesozoic kinematic evolution in the Cameros basin (Iberian Range, NE Sapin) from magnetic subfabrics and mesostructures. Journal of Structural Geology 66, 84-101.

García-Lasanta, C., Oliva-Urcia, B., Román-Berdiel, T., Casas, A.M., Gil-Peña, I., Sánchez-Moya, Y., Sopeña, A., Hirt, A.M., Mattei, M., 2015. Evidence for the Permo-Triassic transtensional rifting in the Iberian Range (NE Spain) according to magnetic fabrics results. Tectonophysics 651-652, 216-231.

García-Lasanta, C., Román-Berdiel, T., Oliva-Urcia, B., Casas, A.M., Gil-Peña, I., Speranza, F., Mochales, T. 2016. Tethyan versus Iberian extension during the Cretaceous period in the eastern Iberian Peninsula: insights from magnetic fabrics. Journal of the Geological Society 173, 127-141.

Gil-Imaz, A., Pocoví, A., Parés, J.M., Lago, M., 2000. Effect of lithostatic pressure and tectonic deformation on the magnetic fabric (anisotropy of magnetic susceptibility) in low-grade metamorphic rocks. J. Geophys. Res. 105, 21305-21317.

Gleizes, G., Nédélec, A., Bouchez, J.L., Autran, A., Rochette, P., 1993. Magnetic susceptibility of the Mont Louis–Andorra ilmenite-type granite (Pyrenees): a new tool for the petrographic characterization and regional mapping of zoned granite plutons. Journal of Geophysical Research 98, 4317–4331.

Gong, Z., van Hinsbergen, D.J.J., Vissers, R.L.M., Dekkers, M.J., 2009. Early Cretaceous syn-rotational extension in the Organya Basin; new constraints on the palinspastic position of Iberia during its rotation. Tectonophysics 473, 3-4, 312-323.

Graham, J.W., 1966. Significance of magnetic anisotropy in Appalachian sedimentary rocks. *In*: The Earth Beneath the Continents. J. S. Steinhart, T. J. Smith (eds.). American Geophysical Union, Geophysical Monographs 10, 627-648.

Grégoire, V., Darrozes, J., Gaillot, P., Nédélec, A., Launeau, P. 1998. Magnetite grain shape fabric and distribution anisotropy vs rock magnetic fabric: a three-dimensional case study. Journal of Structural Geology 20(7), 937-944.

Guimerà, J., Alvaro, M., 1990. Structure et évolution de la compression alpine dans la Rangee Ibérique et la Rangee cotière catalane (Espagne). Bulletin de la Société Géologique de France 6, 2, 339-348.

Guiraud, M., Séguret M., 1984. Releasing solitary overstep model for the Late Jurassic-Early Cretaceous (Wealdien) Soria strike-slip basin (North Spain) In: Biddle KT, Cristhie-Blick N (eds) Strikeslip deformation, basin formation and sedimentation. SEPM Spec Publ 37, 159-175.

Haerinck, T., Adriaens, R., Debacker, T.N., Hirt, A.M., Sintubin, M., 2013. Paramagnetic metamorphic mineral assemblages controlling AMS in low-grade deformed metasediments and the implications with respect to the use of AMS as a strain marker, Journal of the Geological Society 170(2), 263-280.

Hamilton, N., Rees, A.I., 1970. Magnetic fabric of sediments from the Shelf at La Jolla (California). Mar. Geol. 9, M6-M11.

Hansen, A., Chadima, M., Cifelli, F., Brokmeier, H.G., Siemes, H., 2004. Neutron pole figures compared with magnetic preferred orientations of different rock types. Physica B: Condensed Matter 350(1), 120-122.

Hastie, W., Aubourg, Ch., Walkeys, M.K., 2011. Why an “inverse” fabric is no inverse; an integrated AMS-SPO study in MORB like dykes. Terra Nova 23, 49-55.

Hayward, A.B., Graham, R.H., 1989. Some geometrical characteristics of inversion. Geol. Soc. Special Publications 44, 17-39.

Henry, B., 1983. Interprétation quantitative de l’anisotropie de susceptibilité magnétique. Tectonophysics 91, 165-177.

Hirt, A.M., Evans, K.F., Engelder, T., 1995. Correlation between magnetic anisotropy and fabric for Devonian shales on the Appalachian Plateau. Tectonophysics 247, 121-132.

Hirt, A.M., Julivert, M., Soldevilla, J., 2000. Magnetic fabric and deformation in the Navia–Alto Sil slate belt, northwestern Spain. Tectonophysics 320, 1-16.

Housen, B., Richter, C., van der Pluijm, B.A., 1993. Composite magnetic anisotropy fabrics: experiments, numerical models and implications for the quantification of rock fabrics. Tectonophysics 220, 1-12.

Hrouda, F., 1982. Magnetic anisotropy of rocks and its application in geology and geophysics. Geophys. Surveys 5, 37–82.

Hrouda, F., Janak, F., 1976. The changes in shape of the magnetic susceptibility ellipsoid during progressive metamorphism and deformation. Tectonophysics 34, 135-148.

Hrouda, F., Faryad, S.W., Jeřábek, P., Chlupáčová, M., Vitouš, P., 2009. Primary magnetic fabric in an ultramafic body (Moldanubian Zone, European Variscides) survives exhumation-related granulite-amphibolite facies metamorphism. Lithos 111(1), 95-111.

Issachar, R., Levi, T., Lyakhovsky, V., Marco, S., Weinberger, R., 2016. Improving the method of low-temperature anisotropy of magnetic susceptibility (LT-AMS) measurements in air. Geochemistry, Geophysics, Geosystems 17(7), 2940-2950.

Izquierdo-Llavall, E., Casas-Sainz, A.M., Oliva-Urcia, B., 2013. Heterogeneous deformation recorded by magnetic fabrics in the Pyrenean Axial Zone. Journal of Structural Geology 57, 97-113.

Izquierdo-Llavall, E., Román-Berdiel, T., Casas, A.M., Oliva- Urcia, B., Gil-Peña, I., Soto, R., Jabaloy, A., 2012. Magnetic and structural study of the Eaux-Chaudes intrusion: Understanding the Variscan deformation in the western axial zone (Pyrenees). International Journal of Earth Sciences 101 (7), 1817–1834.

Jackson, M., Gruber, W., Marvin, J., Banerjee, S.K., 1988. Partial anhysteretic remanence and its anisotropy: application and grain-size dependence. Geophysical Research Letters 15, 440-443.

Jackson, M., Tauxe, L., 1991. Anisotropy of magnetic susceptibility and remanence: Developments in the characterization of tectonic, sedimentary, and igneous fabric. Reviews of Geophysics 29, 371-376.

Jackson, M., Swanson-Hysell, N.L., 2012. Rock magnetism of remagnetized carbonate rocks: another look. Geol. Soc. London, Spec. Publ. 371, 229–251. doi:10.1144/sp371.3

Jammes, S., Manatschal, G., Lavier, L., 2010. Interaction between prerift salt and detachment faulting in hyperextended rift systems: The example of the Parentis and Mauléon basins (Bay of Biscay and western Pyrenees). AAPG bulletin 94(7), 957-975.

Kelso, P.R., Tikoff, B., Jackson, M., Sun, W., 2002. A new method for the separation of paramagnetic and ferromagnetic susceptibility anisotropy using low field and high field methods. Geophysical

Journal International 151(2), 345-359.

Kissel, C., Barrier, E., Laj, C., Lee, T.Q., 1986. Magnetic fabric in “undeformed” marine clays from compressional zones. Tectonics 5, 769-781.

Kligfield, R., Lowrie, W., Dalziel, I.W.D., 1977. Magnetic susceptibility as a strain indicator in the Sudbury Basin, Ontario. Tectonophysics 40, 3-4, 287-308.

Kligfield, R., 1981. Magnetic susceptibility anisotropy, strain, and progressive deformation in Permian sediments from the Maritime Alps (France). Earth and Planetry Science Letters 55, 1, 181-189.

Kligfield, R., Lowrie, W., Pfiffner, O. A., 1982. Magnetic properties of deformed oolitic limestones from the Swiss Alps; the correlation of magnetic anisotropy and strain. Eclogae Geologicae Helvetiae 75, 1, 127-157.

Kneen, S.J., 1976. The relationship between the magnetic and strain fabrics of some haematite-bearing Welsh slates. Earth and Planetary Sciences Letters 31, 3: 413-416.

Kodama, K.P., Sun, W.W., 1990. SEM and magnetic fabric study of a compacting sediment. Geophysical Research Letters 17(6), 795-798.

Koopman, A., Speksnijder, A., Horsfield, W.T., 1987. Sandbox model studies of inversion tectonics. Tectonophysics 137(1-4), 379-388.

Kratinová, Z., Ježek, J., Schulmann, K., Hrouda, F., Shail, R.K., Lexa, O., 2010. Noncoaxial K-feldspar and AMS subfabrics in the land’s End granite, Cornwall: Evidence of magmatic fabric decoupling during late deformation and matrix crystallization. Journal of Geophysical Research: Solid Earth 115 (B9), 104–125.

Lagabrielle, Y., Bodinier, J.L, 2008. Submarine reworking of exhumed subcontinental mantle rocks: field evidence from the Lherz peridotites, French Pyrenees. Terra Nova 20(1), 11-21.

Lago, M., Gil, A., Arranz, E., Galé, E., Pocoví, A., 2005. Magmatism in the intracratonic Central Iberian basins during the Permian: Palaeoenvironmental consequences. Paleogeography, Palaeoclimatology, Palaeoecology 229, 83-103.

Lanci, L., Zanella, E., 2016. The anisotropy of magnetic susceptibility of uniaxial superparamagnetic particles: Consequences for its interpretation in magnetite and maghemite bearing rocks. J. Geophys. Res. B Solid Earth 121, 27-37.

Larrasoaña, J.C., Pueyo, E.L., Parés, J.M., 2004. An integrated AMS, structural, palaeo- and rock-magnetic study of Eocene marine marls from the Jaca-Pamplona Basin (Pyrenees, N Spain); new insights into the timing of magnetic fabric acquisition in weakly deformed mudrocks. In: Martín-Hernández, F., Lüneburg, C.M., Aubourg, C., Jackson, M. (Eds.) Magnetic Fabrics: Methods and Applications. Geological Society, London. Special Publications 238, 127-144.

Laville, E., Lesage, J.L., Séguret, M., 1977. Géométrie, cinématique, (dynamique) de la tectonique atlasique sur le versant sud du Haut Atlas marocain; aperçu sur les tectoniques hercyniennes et tardi-hercyniennes. Bull. Soc. Géol. France 19, 3 (7), 527–539.

Li, Y.X., Kodama, K.P., 2016. Detecting and correcting for paleomagnetic inclination shallowing of sedimentary rocks: A review. Frontiers in Earth Science 4, 7.

Liesa, C.L., Soria, A.R., Meléndez, A., 2000. Lacustrine evolution in a basin controlled by extensional faults; the Galve Subbasin, Teruel, Spain. AAPG Studies in Geology 46, 295-302.

Liesa, C.L., Simón, J.L., 2009. Evolution of intraplate stress fields under multiple remote compressions: The case of the Iberian Chain (NE Spain). Tectonophysics, 474(1-2), 144-159.

Liesa, C.L., Casas, A.M., Simón, J.L., 2018 La tectónica de inversión en una cadena intraplaca: la Cordillera Ibérica. Revista de la Sociedad Geológica de España (under review).

López-Gómez, J., Arche, A., Marzo, M., Durnad, M., 2005. Stratigraphical and palaeogeographical significance of the continental sedimentary transition across the Permian-Triassic boundary in Spain. Palaeogeography, Palaeoclimatology, Palaeoecology 229, 3–23.

Lowrie, W., 1990. Identification of ferromagnetic minerals in a rock by coercivity and unblocking temperature properties. Geophysical Research Letters 17, 159-162.

Lowrie, W., Hirt, A.M. 1987. Anisotropy of magnetic susceptibility in the Scaglia Rossa pelagic limestone. Earth and Planetary Science Letters 82, 349-356.

Lüneburg, C.M., Lampert, S.A., Lebit, H.D., Hirt, A.M., Casey, M., Lowrie, W., 1999. Magnetic anisotropy, rock fabrics and finite strain in deformed sediments of SW Sardinia (Italy). Tectonophysics 307(1-2), 51-74.

Martín-Chivelet, J., Berástegui, X., Rosales, I., Vilas, L., Vera, J.A., Caus, E., Gräfe, K.U., Segura, M., Puig, C., Mas, R. et al. 2002. Cretaceous. In: Gibbons, W. & Moreno, T. (eds) The Geology of Spain. Geological Society, London, 255-292.

Martín-Hernández, F., Hirt, A.M., 2001. Separation of ferrimagnetic and paramagnetic anisotropies using a high-field torsion magnetometer. Tectonophysics 337(3-4), 209-221.

Martín-Hernández, F., Hirt, A.M., 2003. The anisotropy of magnetic susceptibility in biotite, muscovite and chlorite single crystals. Tectonophysics 367, 13–28. doi:10.1016/S0040-1951(03)00127-6

Martín-Hernández, F., Hirt, A.M., 2004. A method for the separation of paramagnetic, ferrimagnetic and haematite magnetic subfabrics using high-field torque magnetometry. Geophysical Journal International 157(1), 117-127.

Martín-Hernández, F., Kunze, K., Julivert, M. Hirt, A.M., 2005. Mathematical simulations of anisotropy of magnetic susceptibility on composite fabrics. J. Geophys. Res. 110, B06102. doi:10.1029/2004JB003505.

Martín-Hernández, F., Ferré, E.C., 2007. Separation of paramagnetic and ferrimagnetic anisotropies: A review. Journal of Geophysical Research-Solid Earth 112(B3).

Martín-Hernández, F., Dekkers, M.J., Bominaar-Silkens, I.M.A., Maan, J.C. 2008. Magnetic anisotropy behaviour of pyrrhotite as determined by low- and high- field experiments. Geophysical Journal International 174, (1), 42-54.

Masini, E., Manatschal, G., Tugend, J., Mohn, G., Flament, J.M., 2014. The tectono-sedimentary evolution of a hyper-extended rift basin: the example of the Arzacq–Mauléon rift system (Western Pyrenees, SW France). International Journal of Earth Sciences 103(6), 1569-1596.

Mata, M.P., Casas, A.M., canals, A., Gil, A., Pocovi, A., 2001. Thermal history during Mesozoic extension and tertiary uplift in the Cameros Basin, Northern Spain. Basin Res. 13, 91-111.

Mattauer, M., Tapponnier, P., Proust, F., 1977. Sur les mécanismes de formation des chaînes intracontinentales; l'exemple des chaines atlasiques du Maroc. Bulletin de la Société Géologique de France 19, 3, 521-526.

Mattei, M., Sagnotti, L., Faccenna, C., Funiciello, R., 1997. Magnetic fabric of weakly deformed clay-rich sediments in the Italian peninsula: Relationship with compressional and extensional tectonics. Tectonophysics 271, 107-122.

Mattei, M., Speranza, F., Argentieri, A., Rosseti, F., Sagnotti, L., Funiciello, R., 1999. Extensional tectonics in the Amantea basin (Calabria, Italy): a comparison between structural and magnetic anisotropy data. Tectonophysics 307, 33-49.

McClay, K., Dooley, T., 1995. Analogue models of pull-apart basins. Geology 23(8), 711-714.

McCabe, C., Jackson, M., Ellwood, B.B., 1985. Magnetic anisotropy in the Trenton Limestone: Results of a new technique, anisotropy of anhysteretic susceptibility. Geophys. Res. Lett. 12, 333–336. doi:10.1029/GL012i006p00333

Meade, R.H., 1964. Removal of water and rearrangement of particles during compaction of clayey sediments-A review. Geol. Surv. Prof. Pap. 497-B, 23 pp.

Moussaid, B., El Ouardi, H., Casas-Sainz, A., Villalaín, J.J., Román-Berdiel, T., Oliva-Urcia, B., Soto, R., Torres-López, S., 2013. Magnetic fabrics in the Jurassic-Cretaceous continental basins of the northern Central High Atlas (Morocco): geodynamic implications. Journal of African Earth Sciences 87, 13-32.

Muxworthy, A.R., Williams, W., 2004. Distribution anisotropy: the influence of magnetic interactions on the anisotropy of magnetic remanence, in Magnetic Fabric: Methods and Applications, edited by F. Martín-Hernández, C. M. Lüneburg, C. Aubourg and M. Jackson, Geological Soc. Special Pub. 238, 37-47.

Neres, M., Miranda, J. M., Font, E. 2013, Testing Iberian kinematics at Jurassic-Cretaceous times: Tectonics 32 (5), 1312-1319.

Oliva-Urcia, B., Larrasoaña, J.C., Pueyo, E.L., Gil, A., Mata, P., Parés, J.M., Schleicher, A.M., Pueyo, O. 2009. Disentangling magnetic subfabrics and their link to deformation processes in cleaved sedimentary rocks from the Internal Sierras (west central Pyrenees, Spain). Journal of Structural Geology 31, 163-176.

Oliva-Urcia, B., Casas, A. M., Soto, R., Villalaín, J.J., Kodama, K., 2010a. A transtensional basin model for the Organyà basin (central southern Pyrenees) based on magnetic fabric and brittle structures. Geophysical Journal International 184, 1, 111-130.

Oliva-Urcia, B., Rahl, J.M., Schleicher, A.M., Parés, J.M., 2010b. Correlation between the anisotropy of the magnetic susceptibility, strain and X-ray Texture Goniometry in phyllites from Crete, Greece. Tectonophysics 486(1), 120-131.

Oliva-Urcia, B., Román-Berdiel, T., Casas, A.M., Pueyo, E.L., Osácar, C., 2010c. Tertiary compressional overprint on Aptian-Albian extensional magnetic fabrics, North Pyrenean Zone. Journal of Structural Geology 32, 362-376.

Oliva-Urcia, B., Casas, A.M., Ramón, M.J., Leiss, B., Mariani, E., Román-Berdiel, T., 2012. On the reliability of AMS in ilmenite-type granites: an insight from the Marimanha pluton, Central Pyrenees. Geophysical Journal International 189(1), 187-203.

Oliva-Urcia, B., Román-Berdiel, T., Casas, A.M., Bogalo, M.F., Osácar, M.C., García-Lasanta, C., 2013. Transition from extensional to compressional magnetic fabrics in the Cretaceous Cabuérniga basin (North Spain). Journal of Structural Geology 46, 220-234.

Oliva-Urcia, B., Casas, A.M., Moussaid, B., Villalaín, J.J., El Ouardi, H., Soto, R., Torres-López, S., Román-Berdiel, T., 2016. Tectonic fabrics vs. mineralogical artifacts in AMS analysis: A case study of the Western Morocco extensional Triassic basins. Journal of Geodynamics 94-95, 13-33.

Osete, M.L., Gomez, J.J., Pavon Carrasco, F.J., Villalain, J.J., Palencia Ortas, A., Ruiz-Martínez, V.C., Heller, F., 2011. The evolution of Iberia during the Jurassic from palaeomagnetic data. Tectonophysics 502, 1-2, 105-120.

Parés, J.M., 2015. Sixty years of anisotropy of magnetic susceptibility in deformed sedimentary rock. Frontiers in Earth Science 3 (4), 1-13.

Parés, J.M., van der Pluijm, B.A., Dinarès-Turell, J., 1999. Evolution of magnetic fabrics during incipient deformation of mudrocks (Pyrenees, northern Spain). Tectonophysics 307, 1–14.

Parés, J.M., van der Pluijm, B.A., 2002a. Phyllosilicate fabric characterization by low-temperature anisotropy of magnetic susceptibility (LT-AMS). Geophysical Research Letters 29(24).

Parés, J.M., van der Pluijm, B.A., 2002b. Evaluating magnetic lineations (AMS) in deformed rocks. Tectonophysics 350, 283-298.

Parés, J. M., van der Pluijm, B. A., 2004. Correlating magnetic fabrics with finite strain; comparing results from mudrocks in the Variscan and Appalachian orogens. Geologica Acta 3, 213-220.

Parés, J.M., van der Pluijm, B.A., 2014. Low-temperature AMS and the quantification of subfabrics in deformed rocks. Tectonophysics 629, pp.55-62.

Piper, J.D.A., Elliot, M.T., Kneller, B.C., 1996. Anisotropy of magnetic susceptibility in a Palaeozoic flysch basin: the Windermere Supergroup, northern England. Sedimentary Geology 106, 235-258.

Pokorný, J., Suza, P., Hrouda, F., 2004. Anisotropy of magnetic susceptibility of rocks measured in variable weak magnetic fields using the KLY-4s Kappabridge, Geological Society, London, Special Publications 238 (1), 69–76).

Potter, D.K., Stephenson, A., 1988. Single-domain particles in rocks and magnetic fabric analysis. Geophysical Research Letters 15, 10: 1097-1100.

Prior, D. J., Boyle, A.P., Brenker, F., Cheadle, M.C., Day, A., López, G., Peruzzi, L., Potts, G., Reddy, S., Spiess, R., Timms, N.E., Trimby, P., Wheeler, J., Zetterstrom, L., 1999. The application of electron backscatter diffraction and orientation contrast imaging in the SEM to textural problems in rocks. American Mineralogist 84, 1741-1759.

Pueyo Anchuela, Ó., Gil Imaz, A., Pocoví Juan, A., 2012. Factors affecting the record of strain fabrics at the anisotropy of magnetic susceptibility: West-Central South-Pyrenean cleavage domain (Southern Pyrenees; NE Spain). Tectonophysics 554-557, 1-17.

Pueyo Anchuela, O., Ramajo Cordero, J., Gil Imaz, A., Meléndez Hevia, G., 2013. Analysis of anisotropy of magnetic susceptibility in iron-oolitic beds: a potential tool for paleocurrent identification. Int. Journal of Earth Sciences (Geol. Rundsch.) 102, 1131-1149.

Rasmussen, E.S., Lomholt, S., Andersen, C., Vejbæk, O.V., 1998. Aspects of the structural evolution of the Lusitanian Basin in Portugal and the shelf and slope area offshore Portugal. Tectonophysics 300(1-4), 199-225.

Rathore, J.S., 1979. Magnetic susceptibility anisotropy in the Cambrian slate belt of North Wales and correlation with strain. Tectonophysics 53, 1-2, 83-97.

Rathore, J.S., Henry, B., 1982. Comparison of strain and magnetic fabrics in Dalradian rocks from the Southwest Highland of Scotland. Journal of structural Geology 4, 3, 373-384.

Rees, A.I., 1965. The use of anisotropy of magnetic susceptibility in the estimation of sedimentary fabric. Sedimentology 4, 257-271.

Richter, C., Ratschbacher, L., Frisch, W., 1993. Magnetic fabrics, crystallographic preferred orientation, and strain of progressively metamorphosed pelites in the Helvetic Zone of the Central Alps (Qartenschifer Formation). Journal of Geophisical Research 98, 9557-9570.

Richter, C., van der Pluijm, B.A., 1994. Separation of paramagnetic and ferrimagnetic susceptibilities using low temperature magnetic susceptibilities and comparison with high field methods. Physics of the Earth and Planetary Interiors 82, 2, 113-123.

Robion, P., Grelaud, S., Frizon de Lamotte, D. 2007. Pre-folding magnetic fabrics in fold-and-thrust belts: why the apparent internal deformation of the sedimentary rocks from the Minervois basin (NE-Pyrenees, France) is so high compared to the Potwar basin (SW-Himalaya, Pakistan)? Sedimentary Geology 196, 181-200.

Roca, E. 1994. La evolución geodinámica de la Cuenca Catalano-Balear y áreas adyacentes desde el Mesozoico hasta la actualidad. Acta geológica hispánica 29(1), 3-25.

Rochette, P., 1987. Magnetic susceptibility of the rock matrix related to magnetic fabric studies. J. Struct. Geol. 9, 1015-1020.

Rochette, P., Vialon, P., 1984. Development of planar and linear fabrics in Dauphinois shales and slates (French Alps) studied by magnetic anisotropy and its mineralogical control. Journal of Structural Geology 6, 33-38.

Rochette, P., Jackson, M., Aubourg, C., 1992. Rock magnetism and the interpretation of anisotropy of magnetic susceptibility. Reviews of Geophysics 30, 209-226.

Román-Berdiel, T., Pueyo-Morer, E.L., Casas-Sainz, A.M., 1995. Granite emplacement during contemporary shortening and normal faulting: Structural and magnetic study of the Veiga massif (NW Spain). Journal of Structual Geology 17, 1689–1706.

Rosenbaum, G., Lister, G. S., Duboz, C., 2002. Relative motions of Africa, Iberia and Europe during Alpine orogeny. Tectonophysics 359(1-2), 117-129.

Sagnotti, L., Winkler, A., Montone, P., Di Bella, L., Florindo, F., Mariucci, M. T., Marra, F., Alfonsi, L., Frepoli, A., 1999. Magnetic anisotropy of Plio-Pleistocene sediments from the Adriatic margin of the northern Apennines (Italy): implications for the time-space evolution of the stress field. Tectonophysics 311, 139-153.

Salas, R., Casas, A., 1993. Mesozoic extensional tectonics, stratigraphy and crustal evolution during the Alpine cycle of the eastern Iberian basin. Tectonophysics 228, 33–55.

Salas, R., Guimerà, J. 1997. Estructura y estratigrafía secuencial de la cuenca del Maestrazgo durante la etapa de rift Jurásica superior-Cretácica inferior (Cordillera Ibérica Oriental). Boletín Geológico y Minero 108(4-5), 65-74.

Salas, R., Guimerà, J., Mas, R., Martín-Closas, C., Meléndez, A., Alonso, A., 2001. Evolution of the Mesozoic central Iberian Rift System and its Cainozoic inversion (Iberian Range). Peri-Tethys Memoir 6, 145-185.

Sánchez-Moya, Y., Sopeña, A., 2004. 5.3. El Rift Mesozoico Ibérico. In: Geología de España (J.A. Vera, Ed.). SGE-IGME, Madrid. 484-522.

Schmidt, V., Günther, D., Hirt, A.M., 2006. Magnetic anisotropy of calcite at room-temperature.

Tectonophysics 418(1-2), 63-73.

Schmidt, V., Hirt, A.M., Hametner, K., Guenther, D., 2007a. Magnetic anisotropy of carbonate minerals at room temperature and 77 K. American Mineralogist 92, 1673-1684.

Schmidt, V., Hirt, A.M., Rosselli, P., Martín-Hernández, F., 2007b. Separation of diamagnetic and paramagnetic anisotropy by high-field, low-temperature torque measurements. Geophysical Journal International 168, 40-47.

Schmidt, V., Hirt, A.M., Leiss, B., Burlini, L., Walter, J.W., 2009. Quantitative correlation of texture and magnetic anisotropy of compacted calcite–muscovite aggregates. Journal of Structural Geology 31, 1062–1073.

Schwarz, E.J., 1975. Magnetic properties of pyrrhotite and their use in applied geology and geophysics. Paper – Geological Survey of Canada 74-59, 24.

Séguret, M., 1972. Étude tectonique des nappes et series décollées de la partie centrale du versant sud des Pyrénées, in Publ. Ustela, série Géol. Struct. 2, Ustela, Montpellier, 155 pp

Sibuet, J.C., Srivastava, S.P., Spakman, W., 2004. Pyrenean orogeny and plate kinematics. Journal of Geophysical Research: Solid Earth 109(B8).

Simón, J.L., Liesa, C.L., 2011. Incremental slip history of a thrust: diverse transport directions and internal folding of the Utrillas thrust sheet (NE Iberian Chain, Spain). Geological Society, London, Special Publications 349(1), 77-97.

Solum, J.G., van der Pluijm, B.A., 2009. Quantification of fabrics in clay gouge from the Carbonera fault, Spain and implications for fault behavior. Tectonophysics 475, 554-562.

Sopeña, A., López, J., Arche, A., Pérez-Arlucea, M., Ramos, A., Virgili, C., Hernando, S., 1988. Permian and Triassic rift basins of the Iberian Peninsula. In: Triassic-Jurassic Rifting. Developments in Geotectonics, 22-B (Manspeizer, W., Ed.), Elsevier, Amsterdam, 757-786.

Sopeña, A., Sánchez-Moya, Y., 1997. Tectonic systems tract and depositional architecture of the western border of the Triassic Iberian Trough (central Spain). Sediment. Geol. 113, 245–267.

Soto, R., Casas-Sainz, A.M., del Rio, P., 2007a. Geometry of half-grabens containing a mid-level viscous detachment. Basin Research 19, 437-450.

Soto, R., Casas-Sainz, A.M., Villalaín, J.J., Oliva-Urcia, B., 2007b. Mesozoic extension in the Basque-Cantabrian basin (N Spain). Contributions from AMS and brittle mesostructures. Tectonophysics 445, 373-394.

Soto, R. Casas-Sainz, A.M., Villalaín, J.J., Gil-Imaz, A., Fernández-González, G., Del Río, P., Calvo, M., Mochales, T., 2008a. Characterizing the Mesozoic Extension Direction in the Northern Iberian Plate Margin by Anisotropy of Magnetic Susceptibility (AMS*).* Journal of the Geologycal Society 165, 6, 1007-1018.

Soto, R., Villalaín, J.J., Casas-Sainz, A.M., 2008b. Remagnetizations as a tool to analyze the tectonic history of inverted sedimentary basins: a case study from the Basque-Cantabrian basin (north Spain). Tectonics 27, TC1017.

Soto, R., Casas-Sainz, A.M., Villalaín, J.J., 2011. Widespread Cretaceous inversion event in northern Spain: evidence from subsurface and palaeomagnetic data. Journal of the Geological Society 168, 899-912.

Soto, R., Kullberg, J.C., Oliva-Urcia, B., Casas-Sainz, A.M., Villalaín, J.J., 2012. Switch of Mesozoic extensional tectonic style in the Lusitanian Basin (Portugal). Insights from magnetic fabrics. Tectonophysics 536-537, 122-135.

Tarling, D.H., Hrouda, F., 1993. The magnetic anisotropy of rocks. Chapman and Hall. 212p.

Tavani, S., Mencos, J., Bausa, J., Muñoz, J.A., 2011. The fracture pattern of the Sant Corneli-Bóixols oblique inversion anticline (Spanish Pyrenees). Journal of Structural Geology 33, 11, 1662-1680.

Torres-López, S., Villalaín, J.J., Casas, A.M., El Ouardi, H., Moussaid, B., Ruiz-Martínez, V.C., 2014. Widespread Cretaceous secondary remagnetization in the High Atlas (Morocco). A common origin for the Cretaceous remagnetizations in the Western Tethys? Journal of the Geological Society 171, 673-687.

Torres-López, S., Casas, A.M., Villalain, J.J., El Ouardi, H., Moussaid, B., 2016. Pre-Cenomanian vs. Cenozoic folding in the High Atlas revealed by palaeomagnetic data. Terra Nova 28, 2, 91-154.

Tron, V., Brun, J.P., 1991. Experiments on oblique rifting in brittle-ductile systems. Tectonophysics 188, 71-84.

Tugend, J., Manatschal, G., Kusznir, N.J., Masini, E., Mohn, G., Thinon, I., 2014. Formation and deformation of hyperextended rift systems: Insights from rift domain mapping in the Bay of Biscay, Pyrenees. Tectonics 33(7), 1239-1276.

Van der Pluijm, B.A., Ho, N.C., Peacor, D., 1994. High-resolution X-ray texture goniometry. Journal of Structural Geology 16 (7), 1029-1032.

Van der Voo, R., 1969. Paleomagnetic evidence for the rotation of the Iberian Peninsula: Tectonophysics 7, 5-56.

Van Hoorn, B., 1987. Structural evolution, timing and tectonic style of the Sole Pit inversion. Tectonophysics 137, 1-4, 239-284.

Van Wees, J.D., Arche, A., Beijdorff, C.G., López-Gómez, J., Cloetingh, S., 1998. Temporal and spatial variations in tectonic subsidence in the Iberian Basin (E Spain). Tectonophysics 300, 285–310.

Vendeville, B.C., Ge, H., Jackson, M.P.A., 1995. Scale models of salt tectonics during basement-involved extension. Petroleum Geoscience 1(2), 179-183.

Vergés, J., Saura, E. Messager, G., Martín-Martín, J.D., Moragas, M., Razin, P., Grelaud, C., Joussiaume, R., Malaval, M., Hunt, D.W., 2014. Syn to post rift diapirism and minibasins of the central High Atlas (Morocco); the changing face of a mountain belt. Annual Meeting – American Association of Petroleum Geologist 2014.

Villalaín, J.J., Fernández-González, G., Casas, A.M., Gil-Imaz, A., 2003. Evidence of a Cretaceous remagnetization in the Cameros Basin (north Sapin); implications for basin geometry. Tectonophysics 377, 1-2, 101-117.

Villalaín, J.J., Casas-Sainz, A.M., Soto, R., 2015. Reconstruction of inverted sedimentary basins from syntectonic remagnetizations; a methodological proposal. Special Publications, Geological society of London 425, 1, 233-246.

Vissers, R. L. M., Meijer, P., T. 2012. Mesozoic rotation of Iberia: Subduction in the Pyrenees?: Earth-Science Reviews 110, 1-4, 93-110.

Williams, G.D., Powell, C.M., Cooper, M.A., 1989. Geometry and kinematics of inversion tectonics. Geological Society Special Publications 44, 3-15.

Winkler, A., Alfonsi, L., Florindo, F., Sagnotti, L, Speranza, F., 1997. The magnetic anisotropy of rocks: principles, techniques and geodynamic applications in the Italian peninsula. Annali di Geofisica XL, 3, 730-740.

Winklhofer, M., Fabian, K., Heider, F., 1997. Magnetic blocking temperatures of magnetite calculated with a three-dimensional micromagnetic model. J. Geophys. Res. 102, 22695–22709. doi:10.1029/97JB01730

Wood, D.A., Gibson, I.L., 1976. The relationship between depth of burial and mean intensity of magnetization for basalts from eastern Iceland. Geophysical Journal of the Royal Astronomical society 46,2, 497-498.

Worm, H.U., Jackson, M., 1999. The superparamagnetism of Yucca Mountain Tuff. J. Geophys. Res. B Solid Earth 104, 25,415-425,425.

Ziegler, P.A., 1982. Faulting and graben formation in western and central Europe. Phil. Trans. R. Soc. Lond. A, 305(1489), 113-143.

Ziegler, P.A., 1989. Geodynamic model for Alpine intraplate compressional deformation in Western and Central Europe. In: Cooper, M.A., Williams, G.D. (Eds.), Inversion Tectonics, Geological Society Special Publication 44, 63-85.

Ziegler, P. A., 1990. Geological atlas of western and central Europe. Geological Society of London.

Table captions

Table 1. Summary of main characteristics of the basins included in this review as explained in the studies consulted for this review (Ref). Aspects included: geological context and age of the sampled rocks,

sampled lithologies and specific magnetic carriers identified from rock magnetism procedures, basin style controlling the sedimentary infill, tectonic inversion style (presence or lack of detachment level, cleavage development or not), angle between extensional and compressional directions.

Table 2. Summary of the magnetic fabric analyses from each basin included in this review. N sites: number of AMS sites; N samples: total number of analyzed samples; presence or lack of macroscopic cleavage in the studied rocks; analyzed structures other than cleavage; AMS sites and their relationship with the tectonic regime as interpreted in each study; methods of subfabric-analyses used and number of selected sites in which they were applied; methods of magnetic mineralogy analyses and number of selected samples in which they were applied; other non-magnetic methods used that help interpreting the AMS, and number of analyzed samples when specified.

Figure captions

Fig. 1. Location of the Western Tethys inverted extensional basins considered in this review. See for detailed geological cartographies in the respective references.

Fig. 2. Block diagrams representing intraplate geological contexts for basin formation (A) and inversion (B).

Fig. 3. Double ternary diagram showing the key factors intervening in the development of basin inversion styles and classifying the different types of inverted basins. This classification is based on (i) the amount of internal deformation in Y coordinates (i.e., development of mesoscopic cleavage) and (ii) the degree of inversion and type of inversion structures in X coordinates. +Y and –Y correspond to uncleaved and cleaved basins, respectively, the density of cleavage increasing towards the base of the diagram. X coordinates represent an increasing degree of inversion towards -X, from non-inverted, purely-extensional geometries (right corner of the diagram). Three main inversion styles are sketched, from the right to the left: (i) slight inversion of the normal faults bounding the basins with development of open fault-related, hanging-wall anticlines, (ii) folding of the syn-rift units and (iii) development of one or several thrust sheets that are detached into a main pre-rift décollement and transport syn-rift sequences in their hangingwalls.

Fig. 4. Examples of rock magnetism experiments. (A) Thermomagnetic k-T curve of sample LU14-5B of the Mauléon Basin; (B) thermomagnetic k-T curve of sample RS3-13 of the NW Castilian Branch Basin (heating run is represented in red and cooling run in blue, for both a and B); (C) Hysteresis loop of sample VC5-1 (from left to right: uncorrected and corrected for the paramagnetic signal) of the Cabuérniga Basin; (D) IRM acquisition and backfield curves of samples BE5-2 and MO2-3 of the Maestrat Basin; (E) Ratios between the magnetic susceptibility at low and at room temperature (LT/RT) of analyzed samples of Argana Basin. The slopes of 1.5 and 3.8 (perfect paramagnetic) are also plotted.

Fig. 5. Double ternary diagram showing the AMS patterns that can be obtained depending of the

basin/inversion models shown in Fig. 3 and the coaxiality between the resultant magnetic fabrics from extensional and compressional stages. See text for further explanations.

Fig. 6. Paleogeographical sketches of the western Tethys during the Mesozoic (modified after Ziegler, 1990) showing the location of the different studied basins.

Fig. 7. Main sampled units in the different basins: A) NW Castilian Branch Basin: Permo-Triassic red beds (picture of the Tiermes Roman site, where siltstones were excavated as an amphitheater); (B) Maestrat Basin: Lower Cretaceous units (looking West); (C) Cameros Basin: lacustrine marls and limestones of the Enciso Group (looking WNW), the apparent horizontal of non-competent units correspond to ancient terrace farming practices; (D) Nogueres Zone: Triassic units in the forelimb of the Orri sheet; (E) Organyà Basin: Marls of the Lluça Formation in the southern limb of the Santa Fe syncline, affected by normal faults with calcite-filled steps associated with tension gashes (Oliva-Urcia et al., 2010b); (F) Mauléon Basin: Albian black marls; (G) Cabuérniga Basin: Slaty cleavage affecting siltstones; (H) Lusitanian Basin: Upper Triassic units and syn-sedimentary faults; (I) Argana Basin: Permian units (looking West); (J) Aït Attab Basin: Cretaceous red beds; (K) Ouauitzaght Basin: Cretaceous red beds (looking West); (L) Central High Atlas (Imilchil Area): Jurassic marls and limestones.

Fig. 8. Studied basins in the Iberian Range: A) Sketch of the tectonic frame during the Permian-Triassic Iberian Rift in the NW Castilian Branch (see García-Lasanta et al., 2015 for legend details in the geological map); black arrows show the variations of the extension direction along the rift due to strain partitioning processes; B) Interpretation of the spatially distributed incidence of the main tectonic events according to the orientation of magnetic lineations in the Maestrat Basin (from García-Lasanta et al., 2016): green, Iberian extension-related sites; blue, Tethyan extension-related sites; red, Cenozoic compression-related sites; C) Simplified sketches showing the evolution of the extension directions as interpreted from magnetic fabrics along the stratigraphic sequence in the Cameros Basin that points to changes in the boundary conditions of the Iberian plate during Mesozoic. Synthetic stratigraphic column for the sedimentary series in the depocentre of the Cameros Basin as represented in García-Lasanta et al (2014). A, B and C are accompanied by the equal area projection of k_{max} (magnetic lineations) and k_{min} (pole to magnetic foliation) including their density diagrams (blue and red respectively). Data were plotted after restoring bedding to horizontal. Green arrows show the main extension direction.

Fig. 9. Studied basins in the Pyrenees: (A) Restored, intermediate and final stages of geological cross-section in the eastern part of the Nogueres Zone (see Izquierdo-Llavall et al., 2013 for legend details), including representative AMS stereoplots; (B) Extension directions deducted from AMS data during Aptian-Albian in the Organyà Basin, together with lower hemisphere stereographic projection of maximum and minimum susceptibility axes (modified from Oliva-Urcia et al., 2010b); (C) In the upper part, simplified model interpreting a pull-apart basin (under a strike-slip regime) in the Mauléon Basin (Oliva-Urcia et al., 2010a), according to extension directions interpreted from magnetic ellipsoids orientations; in the lower part, simplified model interpreting deformation in the

previous magnetic fabrics due to a NNE–SSW shortening direction during the Pyrenean compression; (D) To the left, cross-section and representative stereoplots of magnetic fabrics in the Cabuérniga Basin; to the right, sketch about the relationships between main structures and AMS characterization (both from Oliva-Urcia et al., 2013).

Fig. 10. Lusitanian and Atlasic studied basins: (A) Rose diagrams representing magnetic lineations orientation (black) and fault trends orientation (grey) for Upper Triassic-Hettangian and Upper Jurassic rocks of the Lusitanian Basin (Soto et al., 2012); (B) Sketch showing extension directions as inferred from AMS data (red arrows) and from faults trend analysis (blue arrows) in the Argana Basin (see Oliva-Urcia et al., 2016 for further information), accompanied by representative AMS stereoplots; (C) Geological map of the Ait Attab Basin and magnetic lineations (k_{max}) orientations after restoration to the horizontal; (D) Geological map of the Ouauitzaght Basin and magnetic lineations (k_{max}) orientations after restoration to the horizontal. (C and D, modified from Moussaid et al., 2013).

Table 1

Studied area	Ref	Structural context	Age	Sampled lithologies	Magnetic carriers	Basin style	Tectonic inversion style (and degree of inversion)	Detachment level	Cleavage	Coaxiality between extension and compression
Mauléon Basin	Oliva-Urcia et al., 2010a	N Pyrenees	Low. Cretaceous	Marls	Phyllosilicates	Strike-slip	Moderate inversion of inherited normal faults. Cleavage-related folding and diapir reactivation in syn-rift units	Pre-extensional detachment (Keuper evaporites)	Strongly cleaved (widespread bedding parallel cleavage + local oblique cleavage)	~45º. N-S extension vs NE-SW compression
Nogueres Zone (Las Paúles Basin)	Izquierdo-Llavall et al., 2013	Axial Pyrenees	Permian-Triassic	Red beds (shales, sandstones and conglomerates)	Phyllosilicates + hematite	Transtension	Strong inversion of inherited normal faults. Folding and southwards tilt of syn-rift units that are involved in a contractional duplex	Pre-extensional décollement within the Paleozoic basement and post-extensional décollement in Late Triassic	Fold-related cleavage	~30º. Radial to NW-SE extension and NNE-SSW Cenozoic compression.
Organyà Basin	Gong et al.,2009; Oliva-Urcia et al., 2010b	Central Pyrenees	Low. Cretaceous	Limestones, marls and marly limestones	Paramagnetic (phyllosilicates)	Transtension/ extension	Moderate inversion of inherited normal faults bounding the basin. Short-cut thrusting and folding of syn-rift units	Pre-extensional detachment (Keuper evaporites)	No cleavage	~60 to 90º. NW-SE to N-S extension vs N-S to NNE-SSW compression
Cabuérniga Basin	Soto et al., 2007b, 2008a; Oliva-Urcia et al., 2013	Basque-Cantabrian Basin	Triassic-Low. Cretaceous	Red beds, limestones, marly limestones and shales	Phyllosilicates + hematite + magnetite	Rift	Weak inversion of inherited normal faults. Open contractional folds + local buttressing and cleavage development	Not detached	No cleavage, incipient cleavage, well-developed cleavage	~60º. Extension is NE-SW during Triassic, Jurassic-Barremian, whereas compression is NNE-SSW
Cameros Basin	Soto et al., 2008a; García-Lasanta et al., 2014	Iberian Range	Triassic-Low. Cretaceous	Siltstones, marls, fine-grained sandstones, red beds, limestones, marly limestones and marls	Phyllosilicates + hematite + magnetite + pyrrhotite	Transtension	Strong inversion of the northern basin boundary (basement faults + shallower extensional décollement at the top of the Triassic). Short-cut thrusting and folding of syn-rift units	Pre-extensional detachment (Keuper evaporites)	No cleavage and cleavage (pre-Cenozoic inversion)	~ 60º. N-S to NE-SW during Triassic, Jurassic-Barremian and Albian, but NW-SE during Aptian
Maestrat Basin	García-Lasanta et al., 2016	Iberian Range	Up. Jurassic-Low. Cretaceous	Mudstones, marls, marly limestones, limestones and fine-grained sandstones	Phyllosilicates + hematite + magnetite + pyrrhotite	Rift	Moderate inversion of the northern basin boundary (basement faults + shallower extensional décollement in the Middle Triassic). Short-cut thrusting and folding of syn-rift units	Pre-extensional detachment (Keuper evaporites) partly reactivated during inversion	No cleavage	~30 to 60º. Extension is NE-SW in the Iberian domain and NW-SE in the Tethyan domain whereas compression is NNE-SSW
NW Castilian Branch Basin	García-Lasanta et al., 2015	Iberian Range	Permian-Triassic	Red beds (mudstones, siltstones and clays)	Hematite + phyllosilicates	Dextral transtension	Weak inversion of inhereted normal faults. Open contractional folds are developed in their hanging-walls	Not detached	No cleavage	~45º. ENE-WSW extension vs NNE-SSW compression
Lusitanian Basin	Soto et al., 2012	W Portugal	Up. Triassic-Jurassic	Siltstones, sandstones and marls	Phyllosilicates + hematite + magnetite	Rift	Weak inversion of inherited normal faults. Open contractional folds + diapir development/reactivation	Pre- to early syn-rift Hettangian salt	No cleavage	~0 to 45º. Radial extension during Triassic and N-S to NE-SW extension during Jurassic. NW-SE Cenozoic compression.
Argana Basin	Oliva-Urcia et al., 2016	Atlas	Triassic	Red sandstones and shales	Phyllosilicates + hematite	Rift	Weak inversion of inherited normal faults. Open contractional folds are developed in their hanging-walls.	Not detached	No cleavage	~45º. WNW-ESE to NW-SE extension vs N-S compression.
Aït Attab Basin	Moussaid et al., 2013	Atlas	Jurassic-Low. Cretaceous	Red beds, calcareous marls	Phyllosilicates + hematite	Transtension	Weak-moderate inversion of inherited normal faults. Open contractional folds in syn-rift units.	Upper Triassic décollement	No cleavage	0º E-W extension vs N-S compression
Ouaouizaght Basin	Moussaid et al., 2013	Atlas	Jurassic-Low. Cretaceous	Red beds, calcareous marls	Phyllosilicates + hematite	Transtension	Weak-moderate inversion of inherente normal faults. Open contractional folds in syn-rift units.	Upper Triassic décollement	No cleavage	0º. E-W extension vs N-S compression
Central High Atlas (Imichil Zone)	Calvín et al., 2018a	Atlas	Jurassic	Limestones	Magnetite + phyllosilicates	Rift	Strong inversion	Upper Triassic décollement	No cleavage and cleaved (axial-plane cleavage)	~30º. NW-SE extension vs N-S compression

Table 1. Summary of main characteristics of the basins included in this review as explained in the studies consulted for this review (Ref). Aspects included: geological

context and age of the sampled rocks, sampled lithologies and specific magnetic carriers identified from rock magnetism procedures, basin style controlling the sedimentary infill, tectonic inversion style (presence or lack of detachment level, cleavage development or not), angle between extensional and compressional directions.

Table 2

Studied area	N sites	N samples	Sites with macroscopic cleavage		Mesostructures	AMS results (N sites)		Subfabric Analyses - Sites	Magnetic mineralogy analyses – Samples	Other methods
			No	Yes (incip./pervas.)		(Sedimentary) Extension related	Tectonic Inversion related			
NW Castilian Branch Basin	55	810	55	0	Joints, tension gashes, normal faults	(9) 37	9	LT-AMS – 5 HF-AMS – 4	k-T curves – 25 IRM – 14	-
Cameros Basin	95	1351	93	2	Syn-sedimentary faults, tension gashes	84	11	LT-AMS – 13 HF-AMS – 8	k-T curves – 28	Thin sections – 10 Calcimetries – 13
Maestrat Basin	42	671	40	2 ("proto")	-	35	7	LT-AMS – 7	k-T curves – 13 hystereses, IRM-back field, IRM three components – 17	Thin sections – 15
Cabuérniga Basin	37	639	29	8	Tension gashes, joints, syn-sedimentary faults	27	10	LT-AMS – 4 AARM – 1	k-T curves, hystereses, IRM – 10	XRD – 6 SEM-EDX – 4
Lusitanian Basin	37	535	36	1	Syn-sedimentary faults	36	1	LT-AMS – 7	M-T curves, IRM-back field, hystereses	-
Nogueres Zone (Las Paúles Basin)	31	540	58	42	Syn-sedimentary faults	8	23	LT-AMS – 3	k-T curves –11	Thin sections
Mauléon Basin	40	720	27 (bedding-parallel)	13 (bedding-oblique)	S0, S1, tension gashes	31	5	LT-AMS – 4	k-T curves – 11 hysteresis – 7	XRD – 14 SEM-EDX
Organyà Basin	45	547	45	0	Tension gashes, faults	28	6	LT-AMS – 8 AARM – 5	k-T curves – 9 hystereses	SEM-EDX calcimetries – 8
Argana Basin	48	Not specified	48	0	Normal faults, fractures, tension gashes	20	Not specified	LT-AMS – 10	k-T curves, hystereses, IRM-back field, IRM three components – 13	EBS-EDX – 2
Aït Attab Basin	20	227	20	0	-	Not specified	Not specified	-	k-T curves, IRM three components	-
Ouaouizaght Basin	22	232	22	0	-	Not specified	Not specified	-	k-T curves, IRM three components	-
Central High Atlas (Imilchil Zone)	53	487	29	0		24	20	LT-AMS AARM – 13	k-T curves	Thin sections

Table 2. Summary of the magnetic fabric analyses from each basin included in this review. N sites: number of AMS sites; N samples: total number of analyzed samples; presence or lack of macroscopic cleavage in the studied rocks; other mesostructures than cleavage analyzed; AMS sites and their relationship with the tectonic regime as interpreted in each study; methods of subfabric-analyses used and number of selected sites in which they were applied; methods of magnetic mineralogy analyses and number of selected samples in which they were applied; other non-magnetic methods used that help interpreting the AMS, and number of analyzed samples when specified.

Figure 1

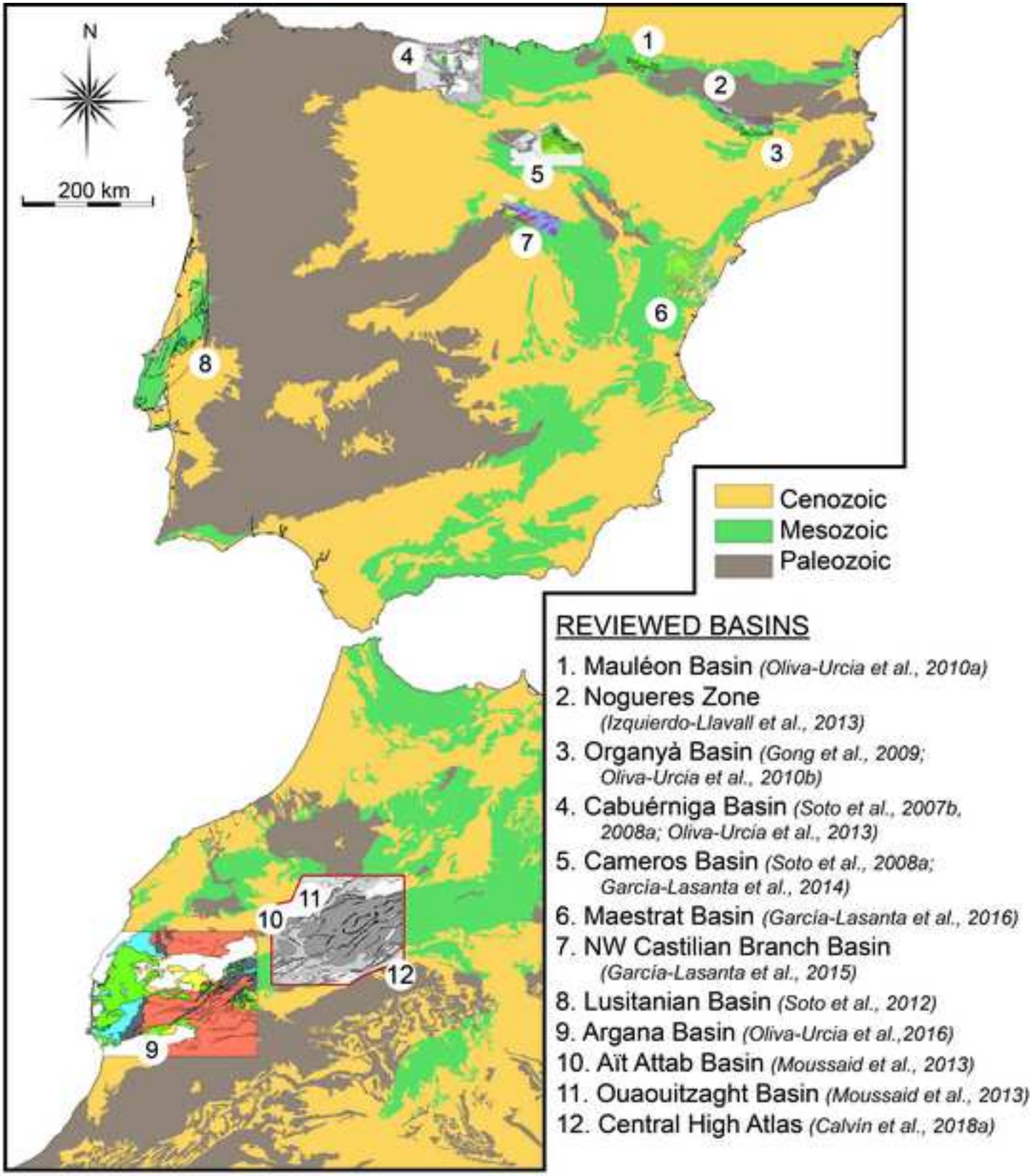

Fig. 1. Location of the Western Tethys inverted extensional basins considered in this review. See for detailed geological cartographies in the respective references.

Figure 2

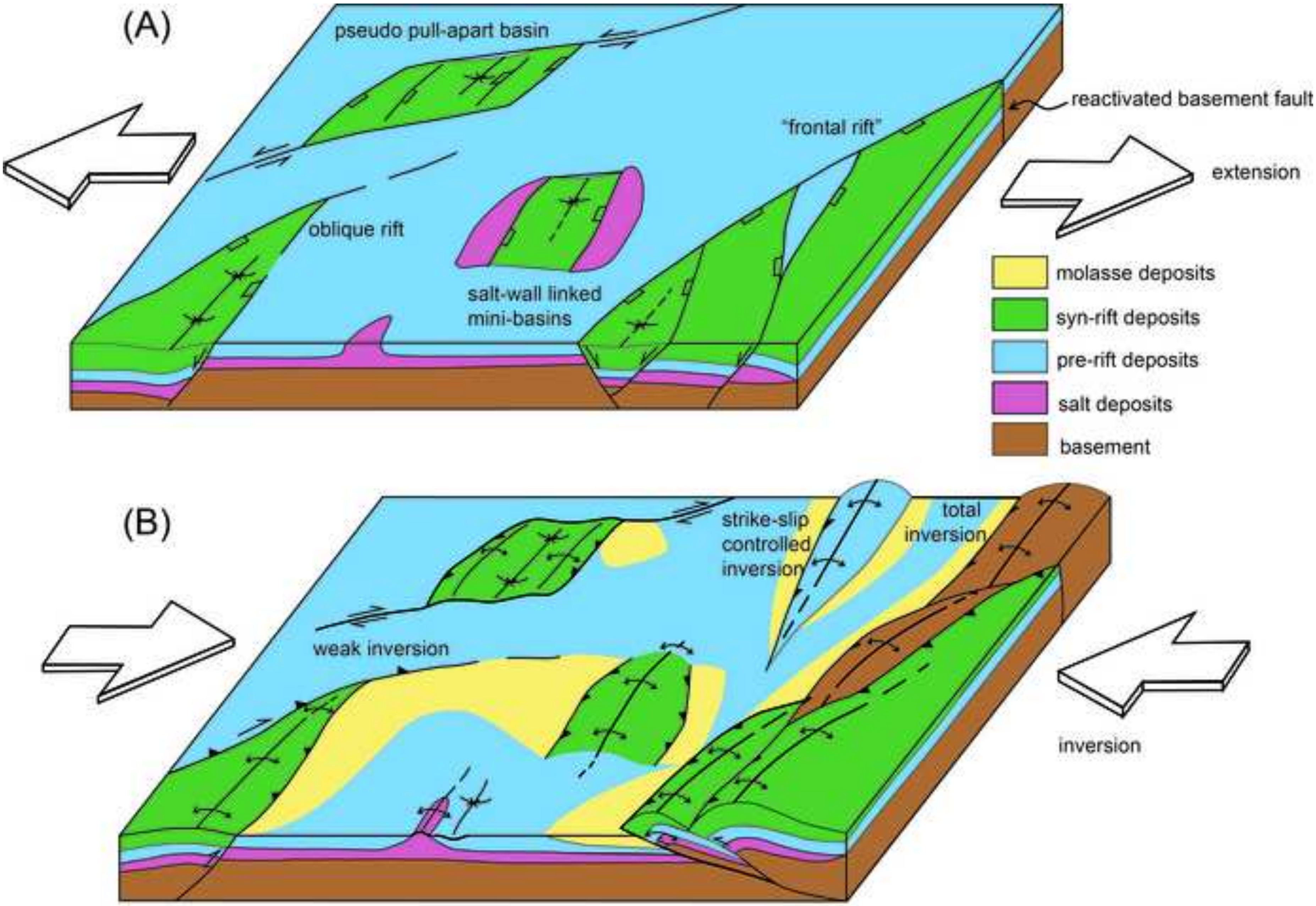

Fig. 2. Block diagrams representing intraplate geological contexts for basin formation (A) and inversion (B).

Figure 3

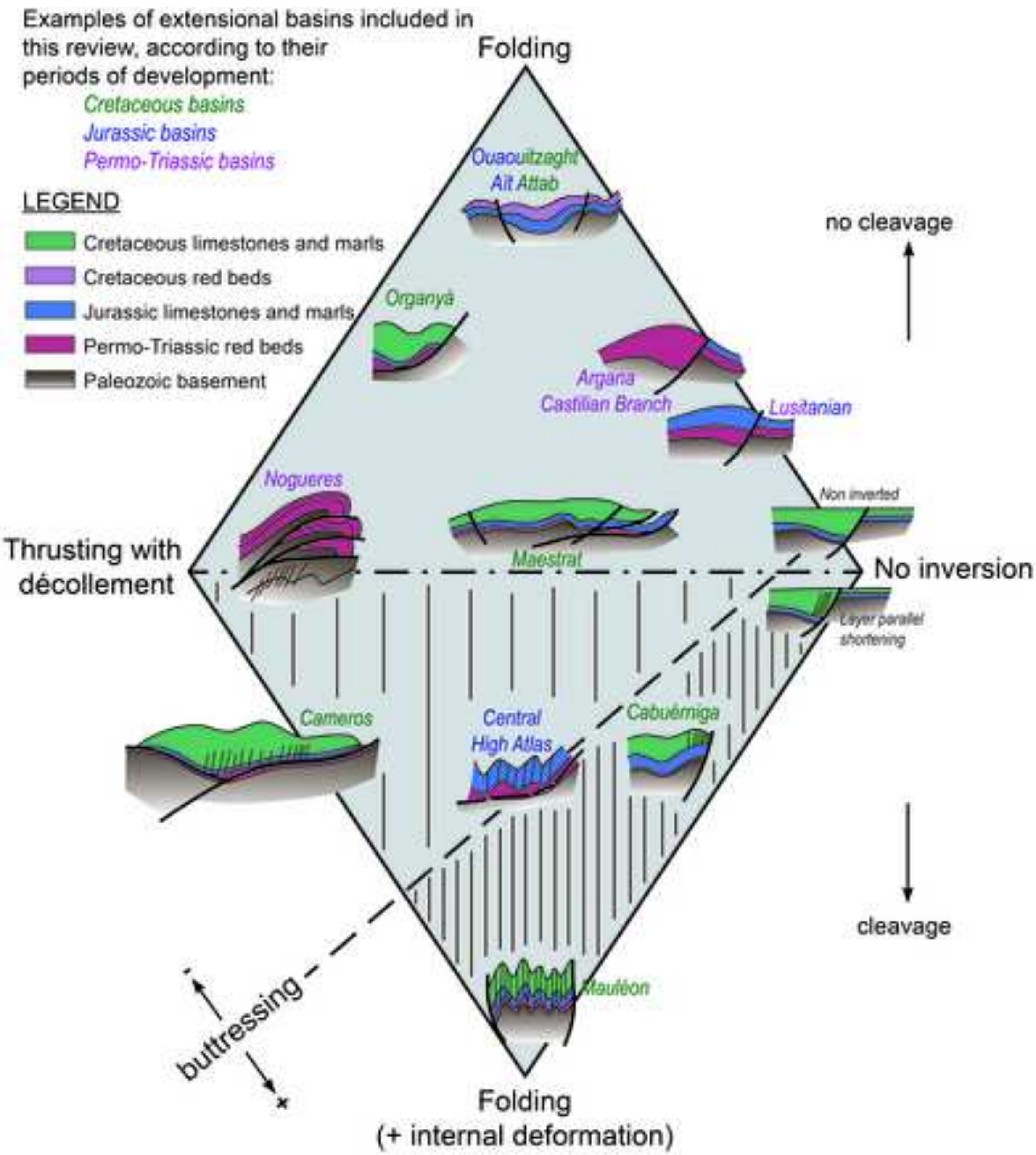

Fig. 3. Double ternary diagram showing the key factors intervening in the development of basin inversion styles and classifying the different types of inverted basins. This classification is based on (i) the amount of internal deformation in Y coordinates (i.e., development of mesoscopic cleavage) and (ii) the degree of inversion and type of inversion structures in X coordinates. +Y and –Y correspond to uncleaved and cleaved basins, respectively, the density of cleavage increasing towards the base of the diagram. X coordinates represent an increasing degree of inversion towards -X, from non-inverted, purely-extensional geometries (right corner of the diagram). Three main inversion styles are sketched, from the right to the left: (i) slight inversion of the normal faults bounding the basins with development of open fault-related, hanging-wall anticlines, (ii) folding of the syn-rift units and (iii) development of one or several thrust sheets that are detached into a main pre-rift décollement and transport syn-rift sequences in their hangingwalls.

Figure 4

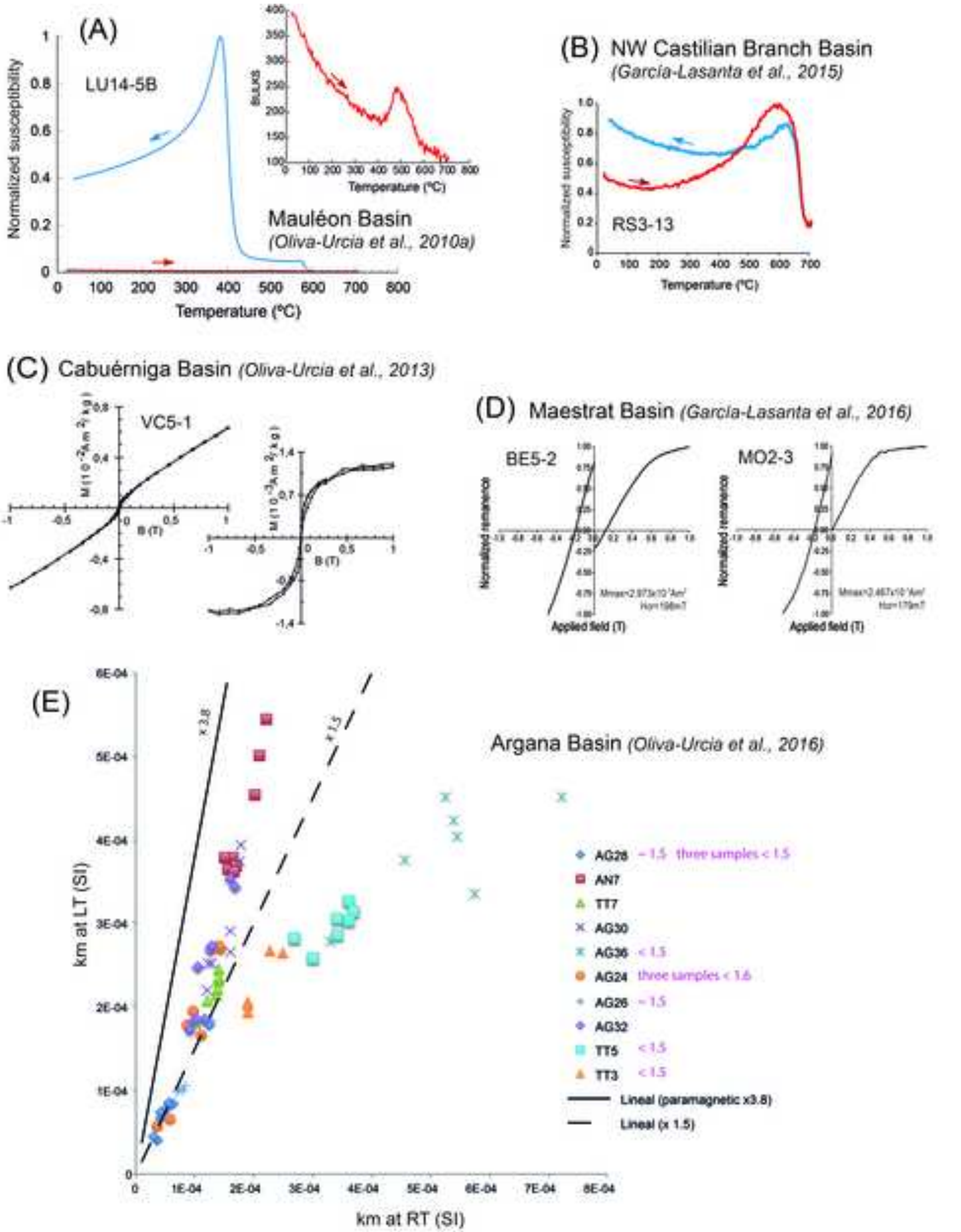

Fig. 4. Examples of rock magnetism experiments. (A) Thermomagnetic k-T curve of sample LU14-5B of the Mauléon Basin; (B) thermomagnetic k-T curve of sample RS3-13 of the NW Castilian Branch Basin (heating run is represented in red and cooling run in blue, for both a and B); (C) Hysteresis loop of sample VC5-1 (from left to right: uncorrected and corrected for the paramagnetic signal) of the Cabuérniga Basin; (D) IRM acquisition and backfield curves of samples BE5-2 and MO2-3 of the Maestrat Basin; (E) Ratios between the magnetic susceptibility at low and at room temperature (LT/RT) of analyzed samples of Argana Basin. The slopes of 1.5 and 3.8 (perfect paramagnetic) are also plotted.

Figure 5

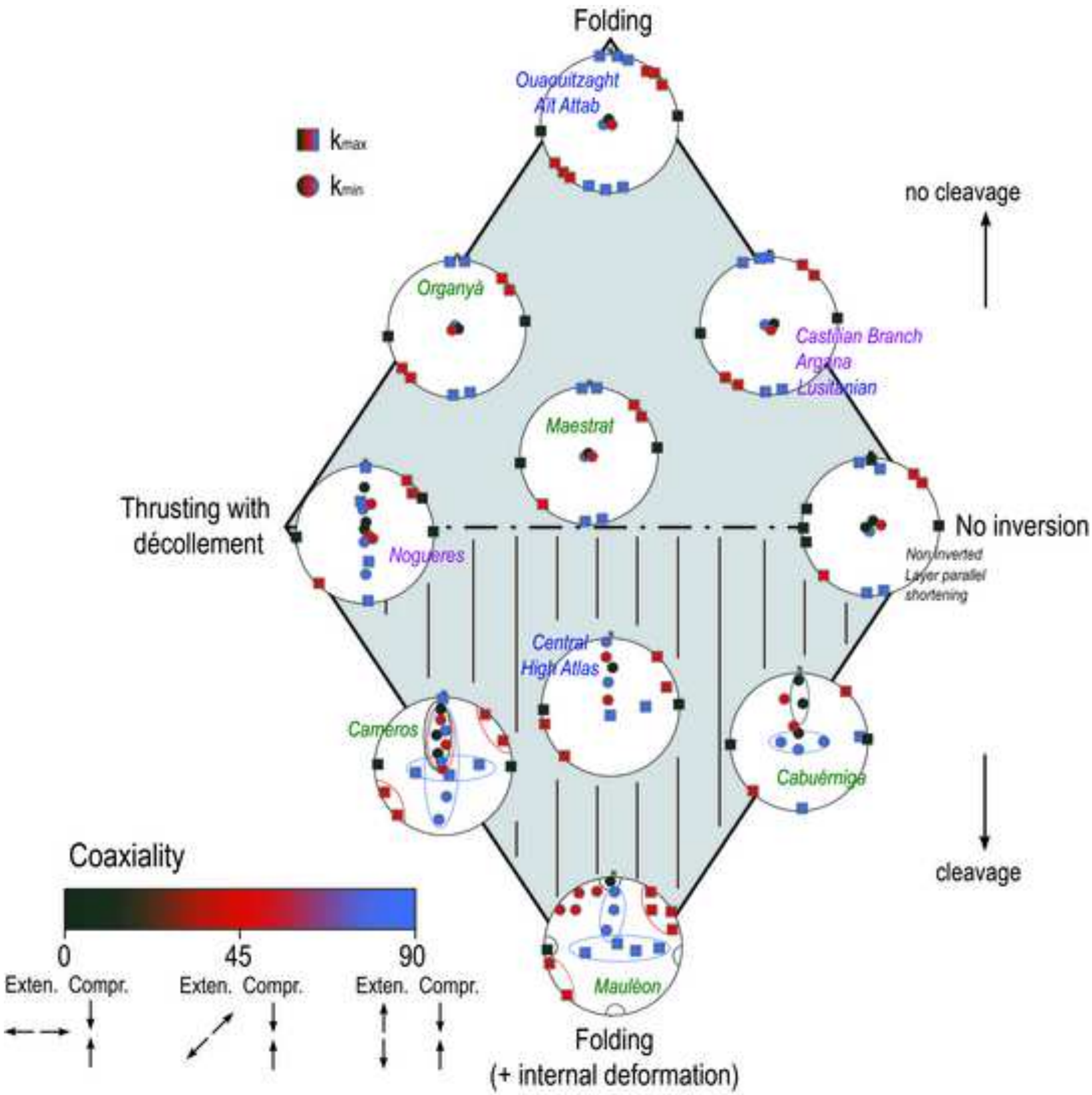

Fig. 5. Double ternary diagram showing the AMS patterns that can be obtained depending of the basin/inversion models shown in Fig. 3 and the coaxiality between the resultant magnetic fabrics from extensional and compressional stages. See text for further explanations.

Figure 6

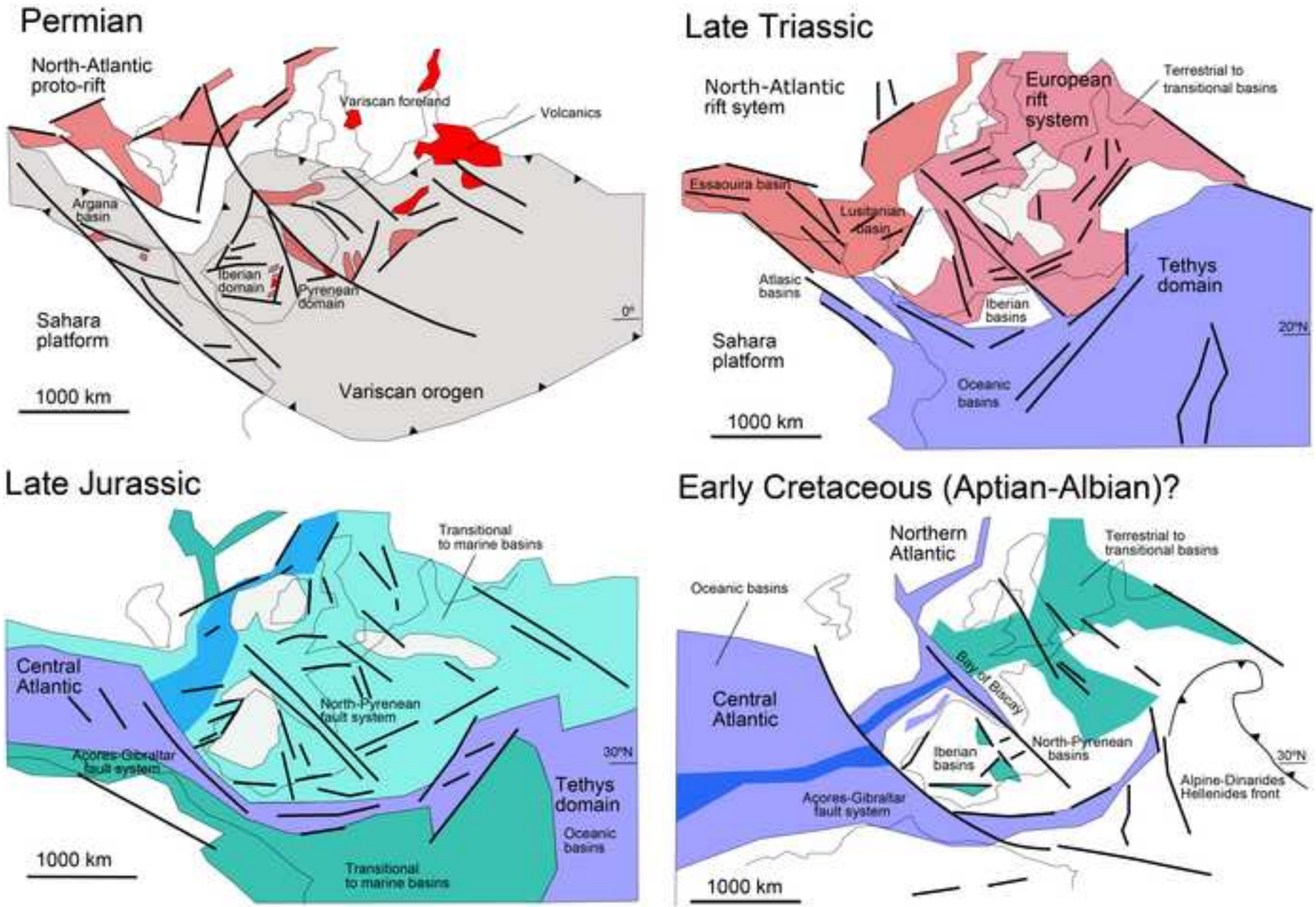

Fig. 6. Paleogeographical sketches of the western Tethys during the Mesozoic (modified after Ziegler, 1990) showing the location of the different studied basins.

Figure 7

Fig. 7. Main sampled units in the different basins: A) NW Castilian Branch Basin: Permo-Triassic red beds (picture of the Tiermes Roman site, where siltstones were excavated as an amphitheater); (B) Maestrat Basin: Lower Cretaceous units (looking West); (C) Cameros Basin: lacustrine marls and limestones of the Enciso Group (looking WNW), the apparent horizontal of non-competent units correspond to ancient terrace farming practices; (D) Nogueres Zone: Triassic units in the forelimb of the Orri sheet; (E) Organyà Basin: Marls of the Lluça Formation in the southern limb of the Santa Fe syncline, affected by normal faults with calcite-filled steps associated with tension gashes (Oliva-Urcia et al., 2010b); (F) Mauléon Basin: Albian black marls; (G) Cabuérniga Basin: Slaty cleavage affecting siltstones; (H) Lusitanian Basin: Upper Triassic units and syn-sedimentary faults; (I) Argana Basin: Permian units (looking West); (J) Aït Attab Basin: Cretaceous red beds; (K) Ouauitzaght Basin: Cretaceous red beds (looking West); (L) Central High Atlas (Imilchil Area): Jurassic marls and limestones.

Figure 8

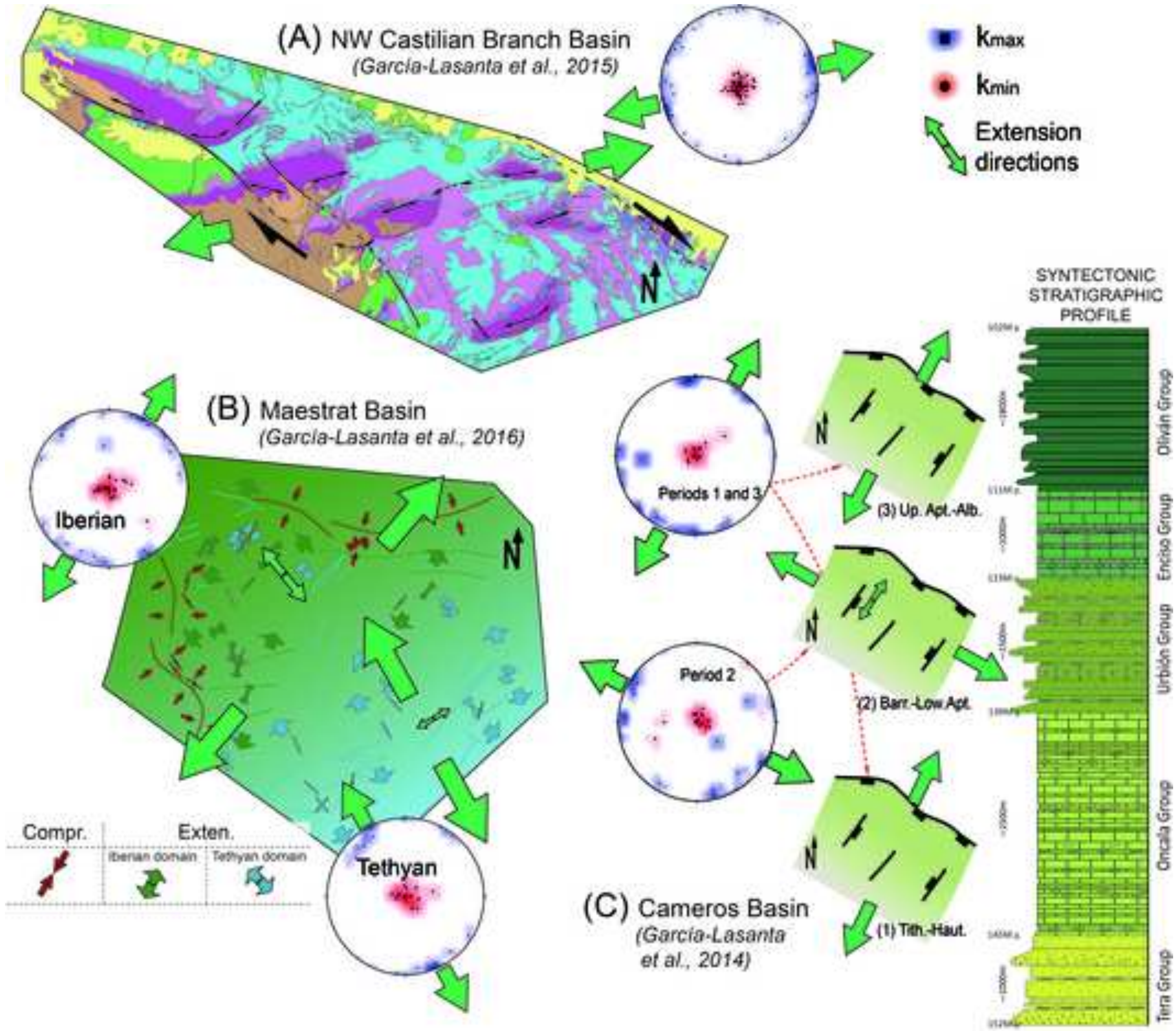

Fig. 8. Studied basins in the Iberian Range: A) Sketch of the tectonic frame during the Permian-Triassic Iberian Rift in the NW Castilian Branch (see García-Lasanta et al., 2015 for legend details in the geological map); black arrows show the variations of the extension direction along the rift due to strain partitioning processes;
B) Interpretation of the spatially distributed incidence of the main tectonic events according to the orientation of magnetic lineations in the Maestrat Basin (from García-Lasanta et al., 2016): green, Iberian extension-related sites; blue, Tethyan extension-related sites; red, Cenozoic compression-related sites; C) Simplified sketches showing the evolution of the extension directions as interpreted from magnetic fabrics along the stratigraphic sequence in the Cameros Basin that points to changes in the boundary conditions of the Iberian plate during Mesozoic. Synthetic stratigraphic column for the sedimentary series in the depocentre of the Cameros Basin as represented in García-Lasanta et al (2014). A, B and C are accompanied by the equal area projection of kmax (magnetic lineations) and kmin (pole to magnetic foliation) including their density diagrams (blue and red respectively). Data were plotted after restoring bedding to horizontal. Green arrows show the main extension direction.

Figure 9

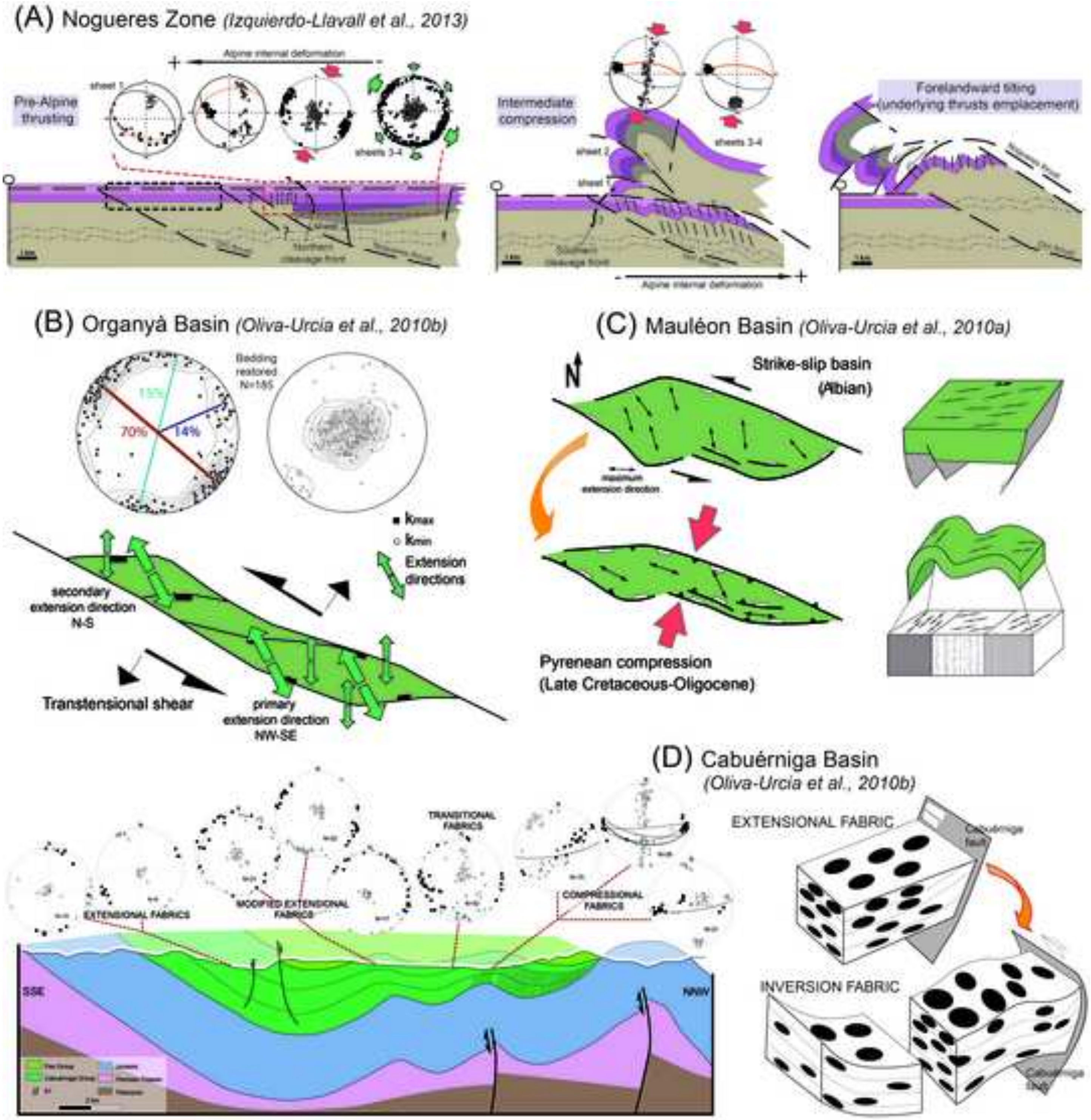

Fig. 9. Studied basins in the Pyrenees: (A) Restored, intermediate and final stages of geological cross-section in the eastern part of the Nogueres Zone (see Izquierdo-Llavall et al., 2013 for legend details), including representative AMS stereoplots; (B) Extension directions deducted from AMS data during Aptian-Albian in the Organyà Basin, together with lower hemisphere stereographic projection of maximum and minimum susceptibility axes (modified from Oliva-Urcia et al., 2010b); (C) In the upper part, simplified model interpreting a pull-apart basin (under a strike-slip regime) in the Mauléon Basin (Oliva-Urcia et al., 2010a), according to extension directions interpreted from magnetic ellipsoids orientations; in the lower part, simplified model interpreting deformation in the previous magnetic fabrics due to a NNE–SSW shortening direction during the Pyrenean compression; (D) To the left, cross-section and representative stereoplots of magnetic fabrics in the Cabuérniga Basin; to the right, sketch about the relationships between main structures and AMS characterization (both from Oliva-Urcia et al., 2013).

Figure 10

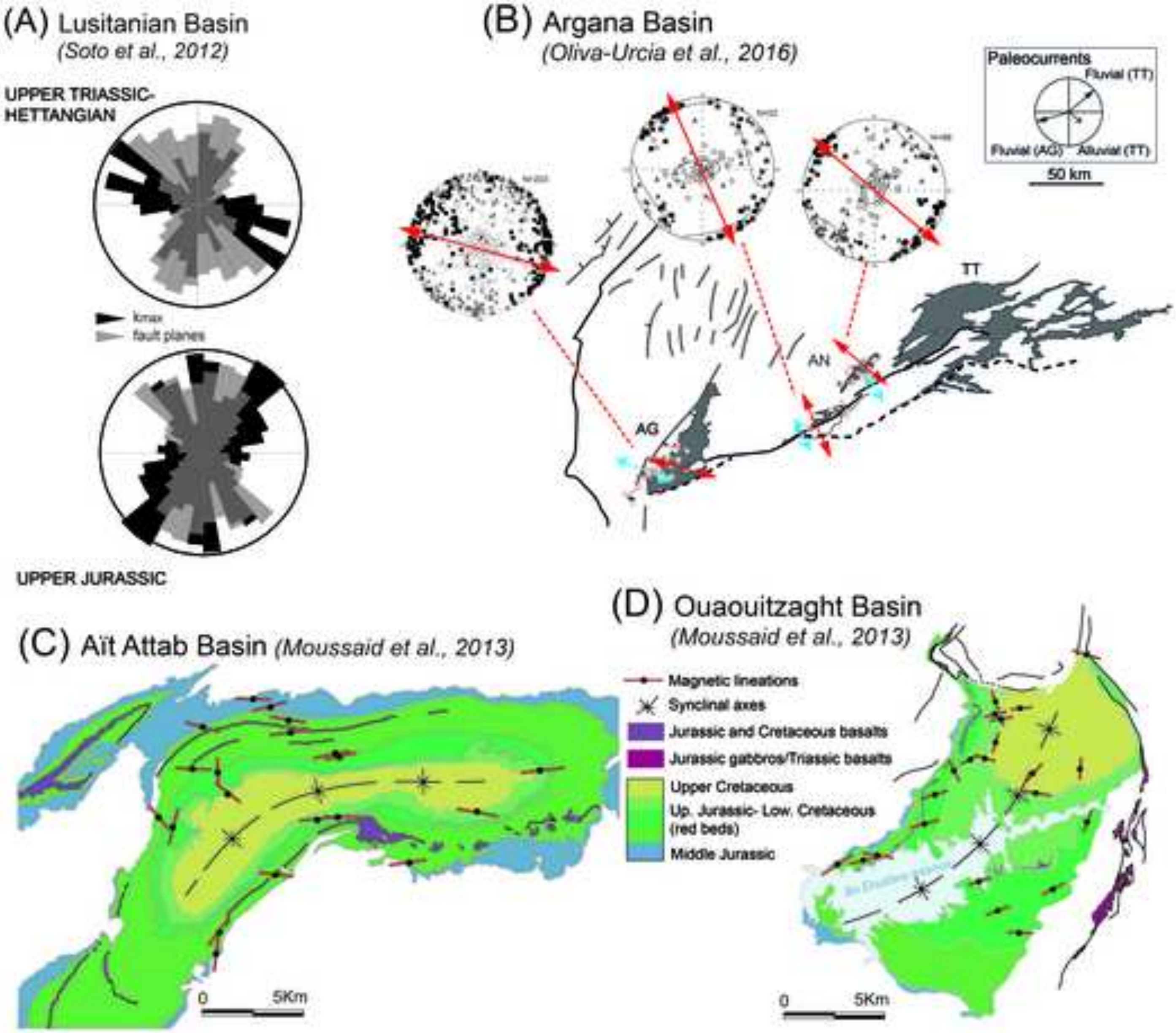

Fig. 10. Lusitanian and Atlasic studied basins: (A) Rose diagrams representing magnetic lineations orientation (black) and fault trends orientation (grey) for Upper Triassic-Hettangian and Upper Jurassic rocks of the Lusitanian Basin (Soto et al., 2012); (B) Sketch showing extension directions as inferred from AMS data (red arrows) and from faults trend analysis (blue arrows) in the Argana Basin (see Oliva-Urcia et al., 2016 for further information), accompanied by representative AMS stereoplots; (C) Geological map of the Ait Attab Basin and magnetic lineations (kmax) orientations after restoration to the horizontal; (D) Geological map of the Ouauitzaght Basin and magnetic lineations (kmax) orientations after restoration to the horizontal. (C and D, modified from Moussaid et al., 2013).